Politecnico di Torino

Corso di Laurea Magistrale in
INGEGNERIA ENERGETICA E NUCLEARE
Collegio di Ingegneria Energetica
Codice Classe **LM-30 (DM270)**
Joint Master of Science Program in Nuclear Engineering (POLY2NUC)

A.A. 2020/2021
Sessione di Laurea ottobre 2021

Design of a module for a 10 MJ toroidal YBCO SMES for the mitigation of PV plants intermittency

Relatore:
Laura Savoldi

Candidato:
Simone Sparacio

Correlatore:
Francesco Laviano

1859

Politecnico
di Torino

Politecnico di Torino

Ringraziamenti

Un sentito grazie a tutte le persone che mi hanno permesso di arrivare fin qui e di portare a termine questo lavoro di tesi.

Grazie alla mia relatrice Laura Savoldi ed al mio correlatore Francesco Laviano, sempre presenti, puntuali e disponibili. Grazie alla loro pazienza e preparazione ho potuto arricchire il mio bagaglio personale ed affrontare quest'ultimo lavoro con serenità e passione.
Grazie ai miei colleghi, ed amici, Sofia e Andrea per i loro fondamentali consigli e per l'appoggio psicologico.

Non posso non menzionare mia sorella ed i miei genitori che da sempre mi sostengono nella realizzazione dei miei progetti. Non finirò mai di ringraziarvi per avermi permesso di arrivare fin qui e per tutto ciò che avete da sempre fatto per me. GRAZIE.

Grazie alla mia seconda famiglia, Teresa, Veronica, e Marco, per aver ascoltato i miei sfoghi ed avermi donato vitali momenti di spensieratezza.

Ed un ultimo immancabile grazie alla mia compagna, che silenziosamente ho sopportato tutti i miei strani atteggiamenti da studente- le nottate in bianco, il parlar da solo a qualsiasi ora per preparare gli esami, i continui affanni ed i momenti di maggior tensione- dandomi tutto il suo amore, sempre e comunque, e tendendomi la mano in ogni difficoltà.

A voi, che mi avete insegnato ad esser forte e a rialzarmi dopo ogni caduta, ad avere il coraggio di vincere ogni sfida, e a diventar in grado di fare della mia vita un capolavoro, dedico questo mio traguardo.

Politecnico di Torino

1859

Abstract

The progressively increasing penetration of electricity from solar photovoltaic plants, needed for a successful deployment of renewable energy sources, strongly depends on the economic cost of system integration, that should also mitigate the intermittency of PV electricity. Among the different available energy storage systems that could be applied to compensate the fluctuating PV power, Superconductive Magnetic Energy Storage (SMES) are attractive because of their high deliverable power and efficiency, and their virtually infinite number of charge-discharge cycles without degradation.

Here we present the design of a module for a 10 MW toroidal YBCO SMES, with a charge/discharge time of 1 s, including the superconducting coil, the power feeding system, and the cryogenic cooling. The design has been performed with a functional analysis approach, translating the system-level requirements into detailed functional and performance requirements for the sub-components, imposing a maximum value for the module radius of 0.5 m and a maximum magnetic self-field of 4 T. The ampere-turn design is based on a stack of 7 commercial 12 mm-width 2G YBCO tapes, with a nominal current of 330 A at 77 K, so that conservatively a total effective current of 1kA at 50 K can be retained for the stack.

For the winding pack of a single module, the optimized design points to a multi-layer coil with radius ~ 0.45 m, wound using 52 layers in parallel, each with 26 turns, with a total inductance of ~2 H and a maximum self-field below 4 T. Nine modules are needed for the entire SMES. Such design is checked by a detailed 2D axisymmetric electro-magnetic model, purposely developed in COMSOL Multiphysics®. The conceptual design of the cryostat is also presented, focusing on the thermal insulation and the cryocooler.

Politecnico di Torino

Summary

List of Figures

List of Tables

Politecnico di Torino

Thesis purpose and layout

This work has been developed in collaboration with the colleagues of the DENERG and the DISAT departments, to conclude my master's degree program in Energy and Nuclear Engineering.

The thesis focuses on the design of a module for a 10 MW toroidal YBCO SMES, with a charge/discharge time of 1 s, including the superconducting coil, the power feeding system, and the cryogenic cooling. The design is based on a very innovative engineering approach called functional analysis, but highlighting peculiar physical aspects, particularly concerning the physics of superconductors.

Chapter 1 gives a brief introduction on the climate changes, focusing on the EU Greenhouse Gases emission, and on the energy transition policies, for framing the overall topic.

Chapter 2 puts in perspective SMES systems as next generation frontier for providing continuity in the power supply. In this chapter the technology is briefly described and some information about possible applications and search fields is provided.

Chapter 3 deals with the Functional Analysis and Allocation approach. It translates system-level requirements into detailed functional and performance requirements for sub-components, by means of a very detailed and comprehensive function tree. The functions are classified into process functions, if they deal directly with the operation of the SMES at the nominal set of parameters, and functions to protect the investment, dealing with the components that should guarantee that any off-normal condition is detected and possibly avoided. Once this procedure gets over, subsystems and components are identified and deeply described.

In Chapter 4 and Chapter 5 both the winding pack and the cryostat are design and validated. A careful bibliography review has been performed in terms of state-of-the-art superconductors, considering pros and cons of both Low Temperature Superconductors (LTS) and High Temperature Superconductors (HTS). Material properties, technological maturity, and cost were the main parameter accounting for. The same approach has been carried out for all the other material (i.e., mandrel, cryostat walls, electrical and thermal insulations, …).

A 2D axisymmetric model based on FEM in COMSOL Multiphysics platform has been built to validate both the design in terms of independent functions, minimum number of cryocoolers needed for keeping the rated temperature, and cool down time.

In Chapter 6 a ‘commonly used’ layout of the power feeding system is introduced and commented. While Chapter 7 is a concluding remark on further perspectives.

1. INTRODUCTION

1.1. There is not a Plane(t) B

Multiple lines of evidence are today indubitably clear on how industrialization has led to a global climate change. One, and the most important, is the dramatic increment of atmospheric CO_2 - reported in Figure 1Figure 2- since the Industrial Revolution [1.1]. Indeed, 97% of climate changes can be ascribed to the greenhouse gases, particularly CO_2, of which 83% is emitted because of fossil fuels.

The future consequences of changing the natural atmospheric greenhouse are difficult to predict, but some effects are clearly visible already today. One among the others is the increase of global mean surface temperature (GMST), which reached 1.18°C in 2020 and have had a very strong impact on organisms and ecosystems.

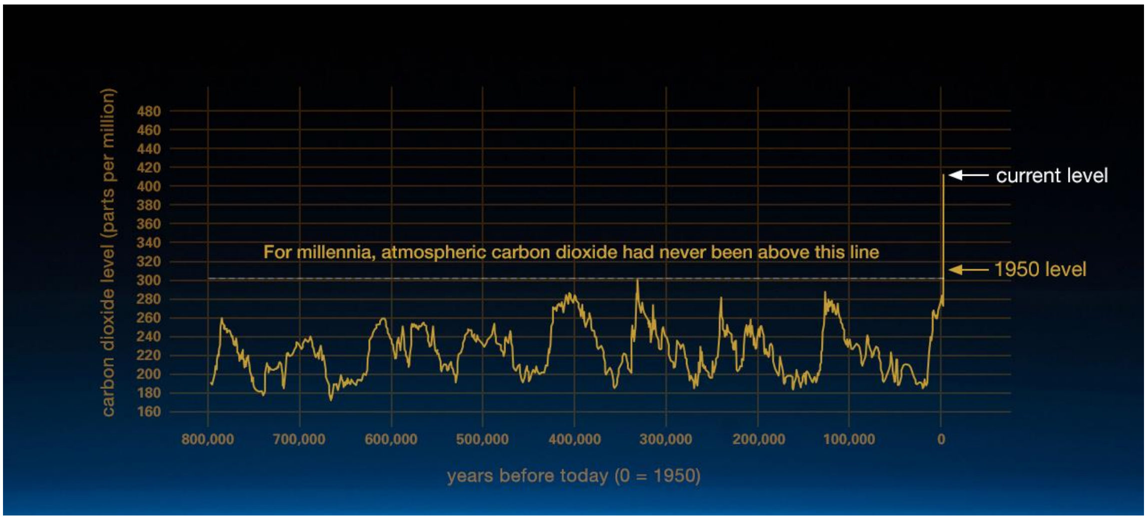

Figure 1. CO_2 emission before and after Industrial Revolution [1.1]

As reported on the Global Status Report [1.4] of the current year, the EU alone, in 2017, has been responsible of 10% of the global CO_2 emissions and, of this, 75% coming from the energy sector. The result has been 283 billion euros spent, in the same year, for economic damages deriving from meteorological catastrophes.

On the base of this tragic situation, the only way out is acting NOW, to enable a future where the environment and living conditions are protected and enhanced. This is called *sustainability*.

1.2. Sustainability means mitigation

Because we are already committed to some level of climate change, responding to these involves a two-pronged approach:

- Reducing emissions of and stabilizing the levels of heat-trapping greenhouse gases in the atmosphere **("mitigation")**,
- Adapting to the climate change already in the pipeline **("adaptation")**.

The first real action taken in this direction was the **Paris Agreement** -the first universal and legally binding agreement on climate change- adopted by 190 parts at the Paris climate conference (COP21) in December 2015.

"The Paris Agreement establishes a global framework for avoiding dangerous climate change by limiting global warming to well below 2ºC and continuing efforts to limit it to 1.5ºC. It also aims to strengthen countries' capacity to address the impacts of climate change and to support them in their efforts" [European Commission].

On July 14, 2019, European Commission adopted a series of proposal to concretize the European policies in terms of climate and energy: the *European Green Deal*. The European Green Deal is a 2050 long-term strategy for zero-net CO_2 emissions. In this contest eight scenarios are analyzed: six promote the use of ***renewable sources*** and the ***energy efficiency***, with different level of penetration, the other two combine ***carbon capture and storage*** for counterbalancing residual emissions. A graph of the foreseen total internal consumption up to 2050, in terms of primary sources, for three different scenarios, is reported in Figure 2.
Today, EU ranks second on the world scale (after China) as annual power increment from renewable sources (Figure 3). The latter are primary wind and solar power, as reported in the *Reference Scenario* of Figure 4, and they will still be growing in future.

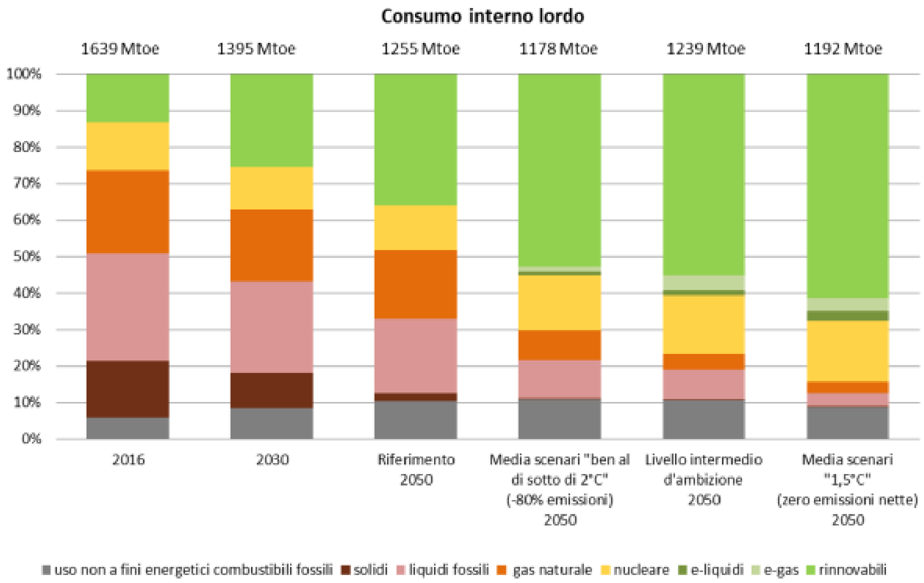

Figure 2. UE gross domestic consumption based on different scenarios [1.2]

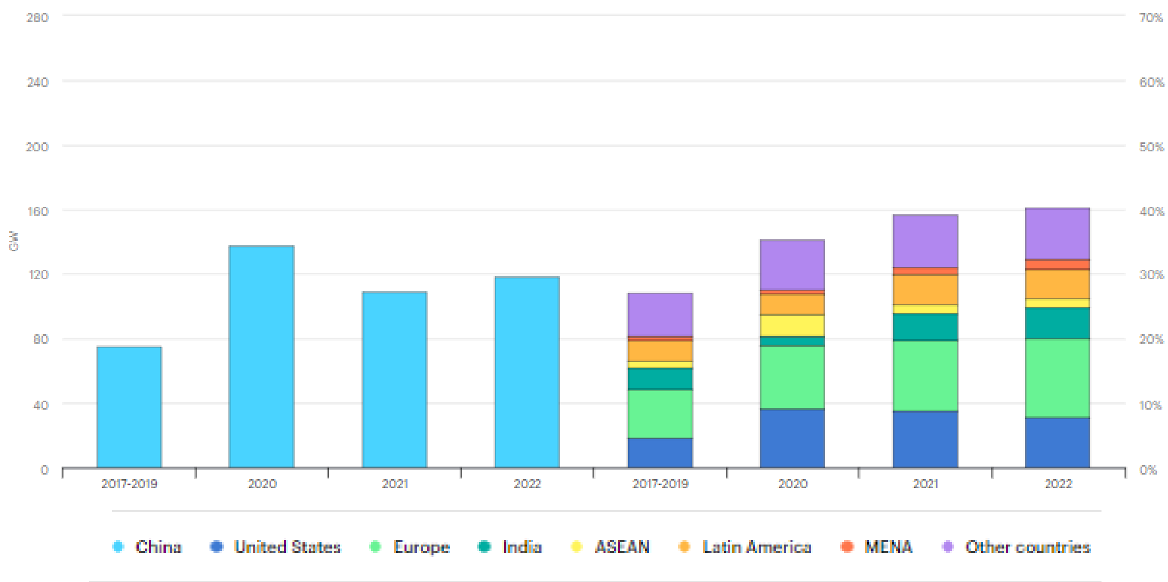

Figure 3. Annual renewable capacity addition in the world, 2017-202

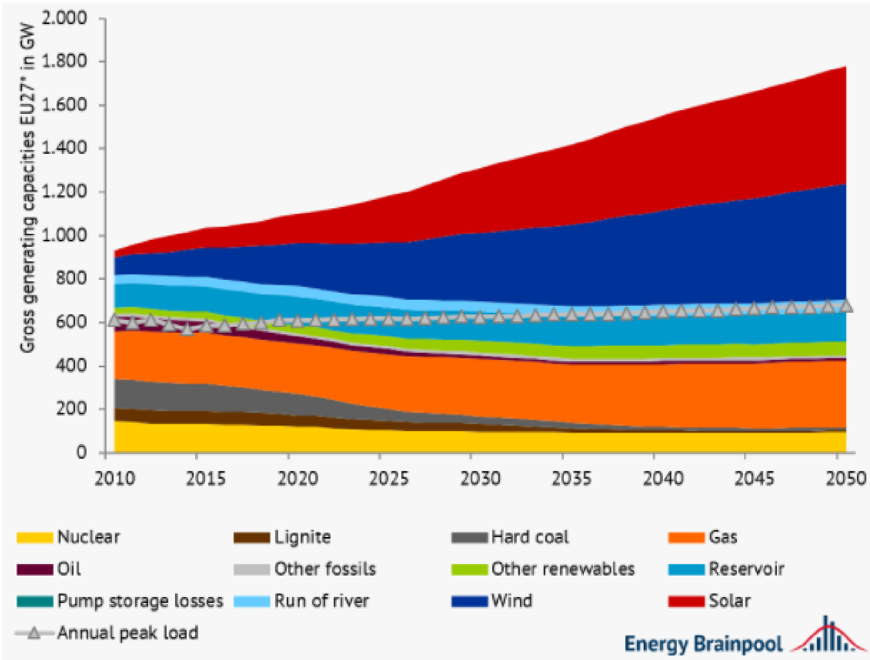

Figure 4. Installed generation capacities in EU 27 (incl. UK, NO and CH) by energy carrier

1.3. Renewable energy intermittency and its impacts on power systems

As the penetration of variable renewable energy (VRE) sources, such as solar (Figure 5) and wind power, increases, maintaining the **reliability of power systems may become more challenging and costly**.

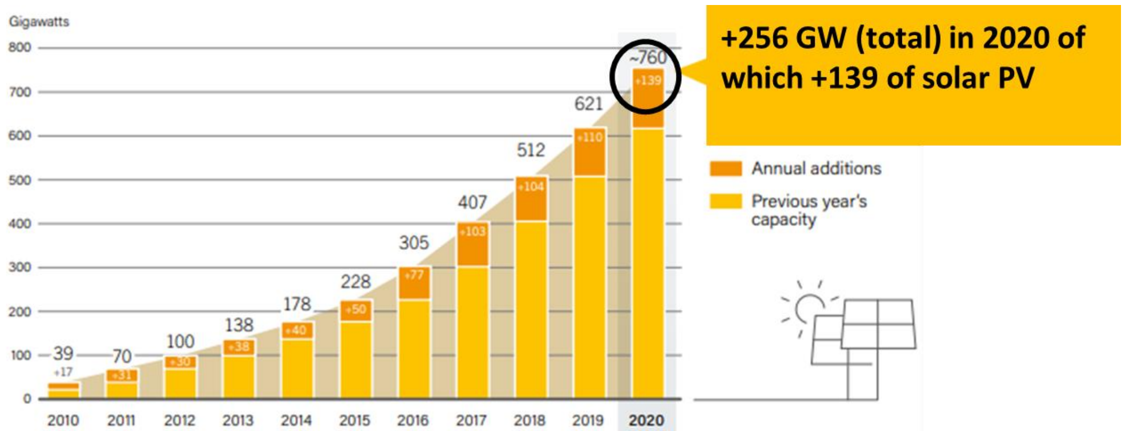

Figure 5. Solar PV global capacity and annual addition, 2010-2020 [1.4]

When supply-demand balance is not maintained, due to the intermittent nature of the variable renewable sources, power system frequencies deviates from steady state values mining system stability and reliability. As result, introduction of harmonic distortion, fault currents, voltage sags, voltage swells, power interruptions and resonance in the system can cause unacceptable power quality distortion.
Policies that promote **energy storage deployment** are then crucial **to balance supply and demand** of renewable generation and minimize the curtailment of electricity.

1.4. Power fluctuation suppression

Among the various approaches, the **implementation of mitigating devices** between the source and the load is by far the most commonly used. A range of power conditioning devices have been developed that can allow a load to ride through a voltage sag or even a complete power interruption. These can be subdivided accordingly to the classification tree of Figure 6 [1.5].
Various types of *Energy Storage System (ESS)* and their possible application depend on the different requirements of industry and community. As shown in Figure 7, there is no single choice that fits all the applications.

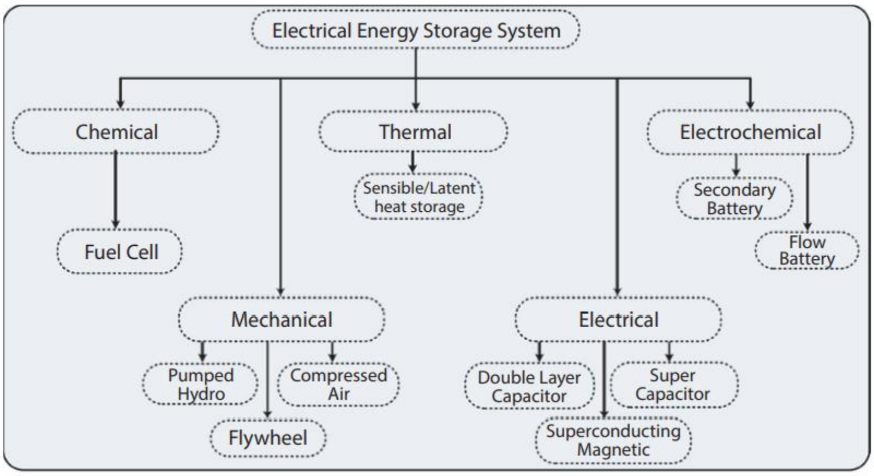

Figure 6. Energy storage technologies classifications [1.5]

Among the different possibilities, **Superconducting magnetic energy storage systems (SMES)** -the only known technology able to store electric energy directly into electric current- are a strongly innovative frontier for providing continuity in the power supply. Indeed, despite their energy density is lower than that of the other energy storage systems (such as battery, double layer capacitor and flywheel), their output power density is about 100 times higher than that of redox flow battery, and about 10 times higher than those of lead acid battery, NaS battery and double layer capacitor [1.9].

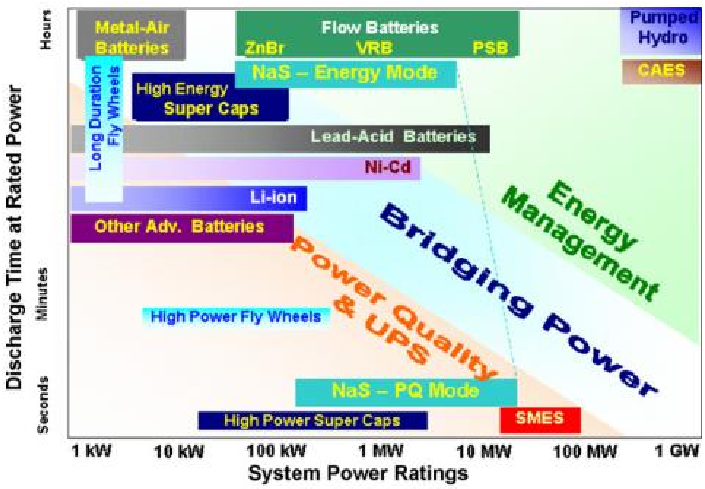

Figure 7. Energy storage systems illustrating storage size and discharge time at rated power [1.9]

1.5. References

[1.1] NASA: Climate Change and Global Warming, Available: https://climate.nasa.gov/evidence/.

[1.2] COMUNICAZIONE DELLA COMMISSIONE AL PARLAMENTO EUROPEO, AL CONSIGLIO EUROPEO, AL CONSIGLIO, AL COMITATO ECONOMICO E SOCIALE EUROPEO, AL COMITATO DELLE REGIONI E ALLA BANCA EUROPEA PER GLI INVESTIMENTI, Bruxelles, 28.11.2018, COM(2018) 773 final.

[1.3] M.H. Albadi, “Solar PV power intermittency and its impacts on power systems – an overview”, Journal of Engineering Research (TJER), Vol. 16, No. 2, pp. 142-150, 2019.

[1.4] Renewable 2021 Global Status Report, Available: https://www.ren21.net/reports/global-status- report/.

[1.5] M. Kathiresh, A. M. Subahani, G.R. Kanagachidambaresan, “Integration of renewable energy sources with smart grid”, Scrivener Publishing LLC, pp. 119–140, 2021.

[1.6] H. A. Mohd, B. Wu, R. A. Dougal, “An overview of SMES applications in power and energy systems”, IEEE Trans. Sustainable Energy, Vol. 1, No. 1, April 2010.

[1.7] X. D. Xue, X. W. E. Cheng, D. Sutanto, “A study of the status and future of superconducting magnetic energy storage in power systems”, Sci. Technol. 19, R31–R39, 2006.

[1.8] Y. Xu, Y. Li, L. Ren, C. Xu, Y. Tang, J. Li, L. Chen, B. Jia, “Research on the application of superconducting magnetic energy storage in microgrids for smoothing power fluctuation caused by operation mode switching”, IEEE Trans. on Applied Supercond., 2018.

[1.9] F. Rahman, S. Rehman, M. Arif Abdul-Majeed, “Overview of energy storage systems for storing electricity from renewable energy sources in Saudi Arabia”, Renewable and Sustainable Energy Reviews, Vol. 16, pp. 274–283, 2012.

[1.10] J. Pahasa, I. Ngamroo, “Coordinated PHEV, PV, and ESS for microgrid frequency regulation using centralized model predictive control considering variation of PHEV number”, DOI: 10.1109/ACCESS.2018.2879982.

[1.11] P. Mukherjee, V.V. Rao, “Effective location of SMES for power fluctuation mitigation of grid connected doubly fed induction generator”, Journal of Energy Storage, Vol. 29, 101369, 2020.

[1.12] W. V. Hassenzahl, D. W. Hazelton, B. K. Johnson, P. Komarek, M. Noe, C. T. Reis, “Electric power applications of superconductivity”, proceedings of the IEEE, Vol. 92, No. 10, October 2004.

[1.13] X. Y. Chen, J. X. Jin, Y. Xin, B. Shu, C. L. Tang, Y. P. Zhu, R. M. Sun, “Integrated SMES technology for modern power system and future smart grid”, IEEE Trans. Applied Supercond., Vol. 24, No. 5, October 2014.

[1.14] A. W. Zimmermann, “Review of the state-of-the-art superconducting magnetic energy storage (SMES) in renewable/distributed energy systems”, CPE 610 Mini Project Final Report.

[1.15] K. E. Nielsen, M. Molinas, “Superconducting magnetic energy storage (SMES) in power systems with renewable energy sources”, DOI: 978-1-4244-6391-6/10/$26.00, IEEE, 2010.

Politecnico di Torino

2. SUPERCONDUCTING MAGNETIC ENERGY STORAGE (SMES)

2.1. Historical overview

SMES were proposed for the first time by Ferrier in 1969-1970, to supply most of the France's cyclic power needs. The original concept was a single, large, toroidal SMES unit, but no work was done beyond the conceptual stage, because it appeared to be economically unfeasible. Although different studies were carried out during the following decade, all came out to the same result: only very large SMES units would be economical [2.1].

Only during 1980, the Electric Power Research Institute (EPRI) first and the Department of Energy (DOE) after funded design improvement and cost reduction study for smaller scales SMES, starting from selected, preferred, previous configuration. The idea was born recognizing that significantly reducing the storage time would increase the economic viability of the technology and that the rapid discharge potential of SMES, together with the relatively high energy related (coil) costs for bulk storage, made smaller systems more attractive. During the following years further studies were conducted, and the first devices start to be built and operated, mainly using Low Temperature Superconductors (LTS) at extremely low temperatures [2.2].

With the discovery of ceramic superconductors with higher critical temperature than conventional metallic superconductors raised, during the last decade of 1900, questions about the possible advantage of using such materials in SMES devices. In 1993 an U.S. project included the investigation of this question, which concluded that the use of high temperature superconductors (HTS) in SMES would result in substantial refrigeration and cost savings [2.3]. Today, several investigators, internationally, are still evaluating the design, cost, and performance impacts of fabricating the SMES coil itself from HTS conductor and simpler refrigeration systems. While SMES currently is only applied in small scale system stability applications, there are however several design and development programs for large-scale SMES plants.

2.2. Technology description

SMES stores energy in the magnetic field created by the flow of direct current in a superconducting coil which has been cryogenically cooled to a temperature below its superconducting critical temperature. Among the different available energy storage systems that could be applied to compensate the fluctuating power of variable renewable energies, and in particular the solar PV one, Superconductive Magnetic Energy Storage (SMES) are attractive because of their high deliverable power (MWs/milliseconds), their efficiency (> 90 %), and their virtually infinite number of charge-discharge cycles without degradation [2.4]. As a result, SMES is expected to become the **next generation technology for storing electrical energy and are part of the road map towards 2050.**

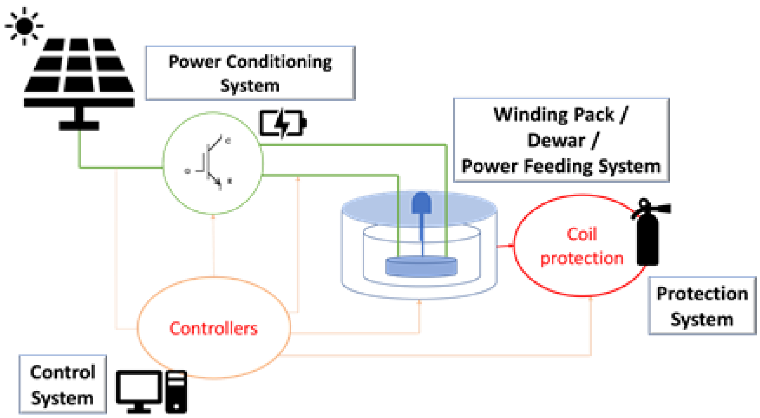

Figure 8. SMES component identification

These devices have a cyclic operation which includes the charge, discharge, and idle work duration (the energy supplied to the grid must be first absorbed from the grid) in power systems.
Figure 8 illustrates the organization of a typical SMES and its main components, but since the core of this thesis relies on the Function Analysis and Allocation approach, a more detailed explanation will be given in the next chapters as logical breakdown of the overall system.

2.3. Possible applications

SMES are becoming so attractive to be part of the road map toward 2050 for future scenarios with CO_2 reduction. A quite complete overview of SMES application in power and energy system, which can be briefly summarized as follow, has been reported in [2.5]:

- **FACTS (Flexible AC Transmission System):** to enhance the controllability and power transfer capability of the grid itself.

- **Load levelling:** to follow system load changes almost instantaneously which provides for conventional generating units to operate at a constant output.
- **Electromagnetic launchers:** to provide high power pulse sources.
- **UPS (Uninterruptible Power Supplies):** to sustain a continuous power supply to certain critical loads protecting them against unexpected power outages as well as over and under voltage conditions.
- **Circuit breaker reclosing:** to reduce the power angle difference across a circuit breaker and allow reclosure of the circuit breaker by briefly supplying some fraction of the power normally transmitted by the transmission line.
- **Spinning reserve:** when a major grid or transmission line is out of service.

For the sake of completeness, Table 1 summaries the outline of SMES for three different applications as proposed by RASMES (Research Association of Superconducting Magnetic Energy Storage) in Japan [2.6].

Table 1. Outline of SMES for power compensation

	Application 1 (Several MWh class)	Application 2 (100 MWh class)	Application 3 (1 GWh class)
Purpose	Frequency control Load fluctuation compensation Generation fluctuation compensation	Load fluctuation leveling (peak cut)	Daily load leveling
Output power	100-200 MW	100-200 MW	100-200 MW
Compensation time	100 seconds	half-1 hour	5-10 hours
Stored energy	3-6 MWh (10-20 GJ)	50-100 MWh (180-720 GJ)	0.5-2 GWh (1.8-7.2 TJ)
Estimation of the required coil numbers for one SMES system. (Assume that half of the total stored energy is available.)			
In a case of assembly with 100 kWh coils	60-120 coils	–	–
In a case of assembly with 1 MWh coils	6-12 coils	100-400 coils	–
In a case of assembly with 10 MWh coils	–	10-40 coils	100-400 coils

In the same study was estimated that the first 1 GWh class SMES for daily load leveling can be installed in the period 2030-40 with a proper integrated operations of several dispersed SMES systems, and that the target cost of SMES of 100 MW output power can be evaluated with 2000 USD/kW.

2.4. Research on SMES

A macroscopic classification about research on SMES system can be split in three main different fields [2.7]:

- **Circuit topology and control techniques of the Power Conversion System (PCS):** depending on the application and the design criteria, three main PCS topologies have been deeply investigated:
  - Thyristor based,
  - Voltage Source Converter (VSC) based,
  - Current Source Converter (CSC) based.
- **Feasible application and control methods:** as anticipated in the previous paragraph.
- **Design and optimization of the superconducting magnets and the cooling system:** regarding the coil design, both the solenoidal and the toroidal configuration are studied and optimized with their own pros and cons [5.3-5.4]. While from the cooling techniques' point of view, recent developments are pushing towards cryogen-free refrigeration systems because of their simplicity and lower cost; however, all the possible cooling methods (i.e., liquid, solid, mixed) are still considered in this field [5.2].

2.5. References

[2.1] W. V. Hassenzahl, "Superconducting magnetic energy storage", Proceedings of the IEEE, Vol. 71, No. 9, September 1983.

[2.2] R. J. Loyd, S. M. Schoenung, T. Nakamura, "Design advances in superconducting magnetic energy storage for electric utility load leveling", IEEE Trans. on Magnetics, Vol. 23, No. 2, March 1987.

[2.3] S. M. Schoenung, "Survey of U.S. SMES development programs", Applied Supercond., Vol.1. No. l-9, pp. 1443-1455, 1993.

[2.4] Md. A. Al Zaman, S. Ahmed, N. J. Monira, "An overview of superconducting magnetic energy storage (SMES) and its applications", International Conference on Nanotechnology and Condensed Matter Physics, , BUET –Dhaka, Bangladesh, Jan 2018.

[2.5] Kondoh et al., "Electrical energy storage systems for energy networks," Energy Conversion and Management, Vol. 41, No. 17, pp. 1863– 1874, Nov. 2000.

[2.6] S. Nomura, T. Shintomi, S. A. Fellow, T. Nitta, R. Shimada, S. Meguro, "Technical and cost evaluation on SMES for electric power compensation", IEE Trans. Applied Superconductivity, Vol. 20, No. 1373-1378, 2010.

[2.7] X. D. Xue, K. W. E. Cheng, D. Sutanto, “A study of the status and future of superconducting magnetic energy storage in power systems”, Supercond. Sci. Technol. 19, R31–R39, 2006.

[2.8] J. Zhu, M. Qiu, B. Wei, H. Zhang, X. Lai, W. Yuan, “Design, dynamic simulation and construction of a hybrid HTS SMES (high-temperature superconducting magnetic energy storage systems) for Chinese power grid”, Energy Vol. 51, pp. 184-192, 2013.

Politecnico di Torino

3. FUNCTIONAL ANALYSIS AND ALLOCATION APPROACH

Functional Analysis and Allocation is a top-down process of translating system-level requirements into detailed functional and performance design criteria. The result of the process is a defined Functional Architecture with allocated system requirements that are traceable to each system function.
The goal of requirements analysis is to determine the needs that make up a system to satisfy an overall need and to comply a set of operating constraints. The output of the Requirements Analysis is a set of top-level functional definitions and accompanying performance and design requirements which become the starting point of the Functional Analysis and Allocation. The second step is to identify the lower-level functions required to perform the various system functions. As this is accomplished, the system requirements are allocated, and functional architecture is developed [3.1-3.2]. The function tree is presented in Figure 9: the functions are classified into process functions, if they deal directly with the operation of the SMES at the nominal set of parameters, and functions to protect the investment, which deal with the components that should guarantee that any off-normal condition is detected and possibly avoided.
Finally, the design phase requires the identification of an operational mode of the system as reference for the analysis (e.g., cool down, nominal condition, off-normal operation, etc.), as the same component may accomplish different functions depending on the operational mode.

3.1. Process functions

The two main process functions of a SMES system are the absorption and the release of electric power within fraction of cycle and the storage of magnetic energy for long time and with high efficiency. Below these ‘top level’ functions, a series of ‘lower-level’ ones can be identified on a general ground and on a more detailed perspective, depending on the specific application. For instance, it must be able to supply uninterruptible power during short time interruption of the grid supply, to compensate the reactive power demand, to smooth the pulsating load, and to reduce the harmonic pollution of the grid. Moreover, it must guarantee the continuous current flowing to be within superconducting windings and ensure the continuous connection with the power supplier/absorber. To satisfy these functions, a suitable number of turns and layers must be ensured for the superconducting pack and a proper insulation must be sized for withstanding over-voltages across each turn, each layer, and between the coil and the

environment. Moreover, a cryogenic system must be foreseen to keep the rated temperature and it must be design in order to guarantee mechanical and thermal anchoring of the system while a system of current leads must guarantee the electrical connection of the SC coil to the grid.
All the related sub-systems and components are designed in such a way that each constitutive component full-fills its own independent function and its own constraints.

3.2. Functions to protect the investment

The safety and the integrity of the whole system should be guaranteed by proper functions to protect the investments. They integrate the control and protection system requirements in terms of detecting and possibly avoiding any abnormal conditions, protecting the mildest components, and ensuring the required work compliance.

3.3. Subsystems and components identification

SMES system can now be subdivided into the following subsystems, reported in Figure 5, able to satisfy each of the independent function identified in the previous functional analysis:

1. **Power conditioning system (PCS):** for regulating the electricity exchange between the SMES and the grid – it converts the current from AC to DC, and vice versa, and charges and discharges the coil. It is commonly composed by a *multi-phase transformer*, a multi-*phase inverter* (that can be used as active filter), a *DC-link capacitor* (to stabilize a proper voltage level for the correct operation of the inverter), a *four-quadrant chopper* (for converting the fixed DC voltage to a variable DC voltage), and a *switch* (for interrupting the circuit in case of abnormal conditions and discharging the SMC).
2. **Winding Pack (WP):** for storing the magnetic energy without joule losses (excluding those in charge/discharge mode operation). It is composed by the *superconducting coil*, a proper sized *insulation* (for withstanding over-voltages), and a *mandrel* (for the structural stability of the magnet).
3. **Dewar:** that includes: a *cryostat*, which walls must offer excellent thermal insulation in order to minimize heat flow into the cryogenic region, and a *cryogenic auxiliary system* which maintains the coil temperature below the critical temperature of the superconductor. In chapter 5 the cryostat will be further subdivide in functional independent subcomponents as described in the previous function tree.

4. **Power Feeding System:** to guarantee, by means of s*uperconducting terminations and current leads*, electrical connections to the power supplier/absorber and the grid.
5. **Control and protection system**: for establishing a link between power demands from the grid and power flow to or from the SMES coil. It receives dispatch signals from the power grid and status information from the SMES coil, the refrigerator, and from other equipment. It also detects and protects the system from any abnormal condition that may cause safety hazard to personnel or damage the magnet.

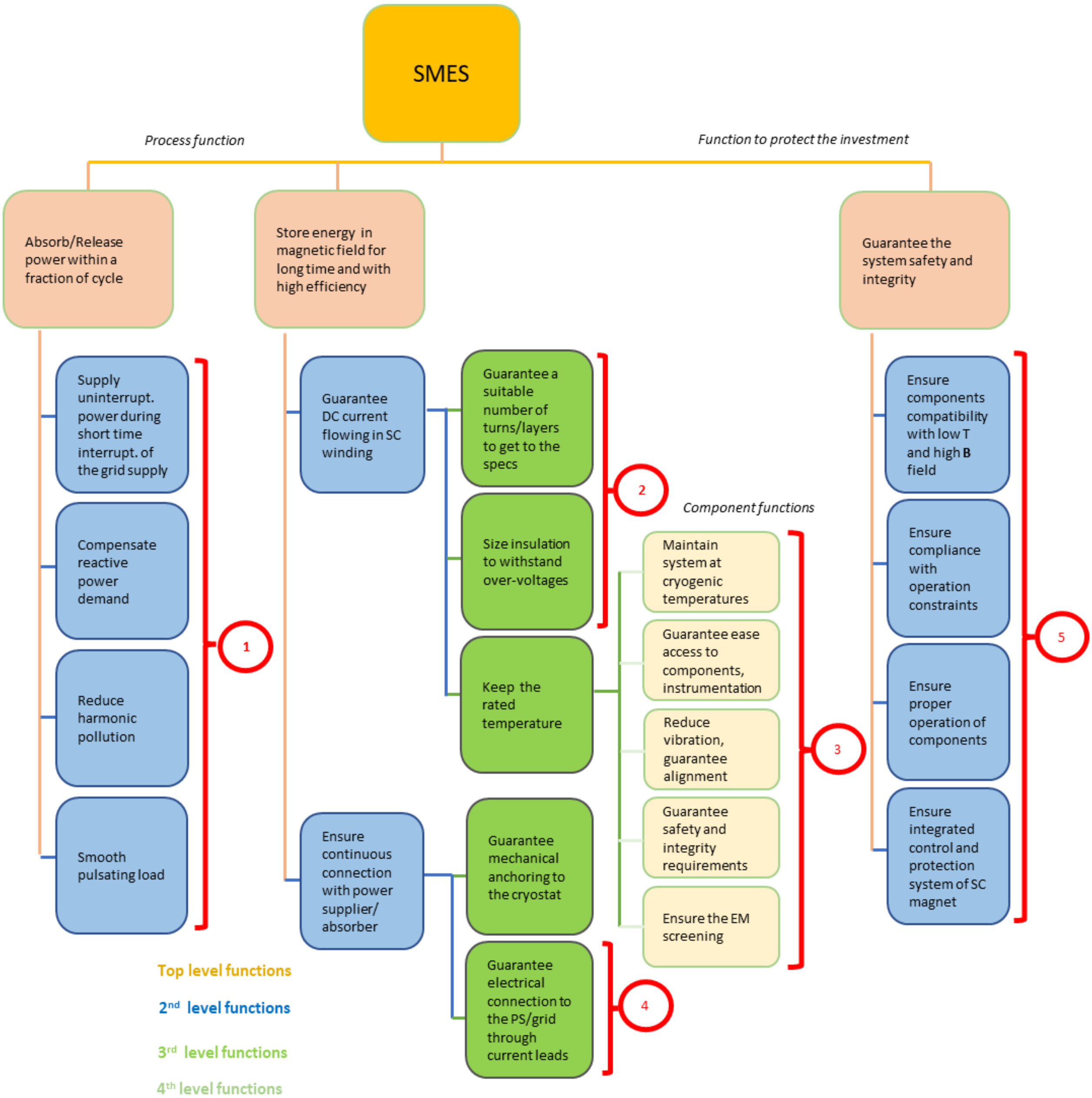

Figure 9. SMES function tree: 1 = Power Conditioning System; 2 = Winding Pack; 3 = Dewar; 4 = Power Feeding System; 5 = Control and Protection System

3.4. References

[3.1] R. Bonifetto, N. Pedroni, L. Savoldi, R. Zanino, “Identification of the postulated initiating events of accidents occurring in a toroidal field magnet of the EU DEMO”, ISSN: 1536-1055 (Print) 1943-7641 (Online) Journal homepage: https://www.tandfonline.com/loi/ufst20.

[3.2] D. Henry, M. Chalifour, A. Forgeas, V. Kalinin, E. Monneret, L. Serio, G. Vincent, T. Voigt, “Process flow and functional analysis of the ITER cryogenic system”, AIP Conference Proceedings 1218, 676 (2010).

Politecnico di Torino

4. WINDING PACK DESIGN

The winding pack is the first identified sub-system. As already stated, the design of the winding pack must guarantee a suitable number of turns/layers to get to the required specifications, a proper sized insulation to withstand normal and off-normal over-voltages and a continuum electrical connection to the PS/grid by means of terminations. The WP can then be split into three sub-components, the *multi-layer multi-turn SC stack*, the *electrical insulation and the terminations*, as reported in Figure 10.

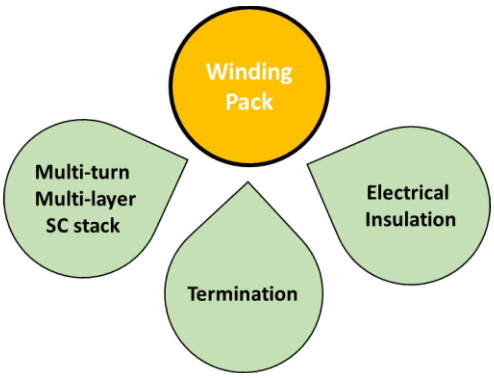

Figure 10. Winding Pack breakdown analysis

4.1. Methodology

One of the main goals when designing a SMES is to maximize the stored energy while minimizing the volume of the coil (i.e., minimizing the required amount of superconducting material and the cost itself). The maximum stored energy is determined by two factors:

- The characteristics of the conductor, which determines the maximum current (superconductors carry substantial currents in high magnetic fields),
- The size and geometry of the coil, which determines the inductance of the coil (i.e., the larger the coil, the greater the stored energy).

Equation (1) gives the basis for superconducting magnetic energy storage.

$$E = \frac{1}{2} L I^2 \tag{1}$$

Where:

- E is the stored magnetic energy (J)
- I is the operating current (A)
- L is the coil self-inductance (H)

Despite the simplicity of this formulae, most of the present design turns around it, and three successive steps have been logically analyzed as discussed in the following paragraphs.

4.1.1. Choice of the superconductor

Perfect conductivity and perfect diamagnetism are the keys parameter of superconductors. Their behavior and the critical limits are commonly represented in the temperature-magnetic field-current density phase space, reported in Figure 11.

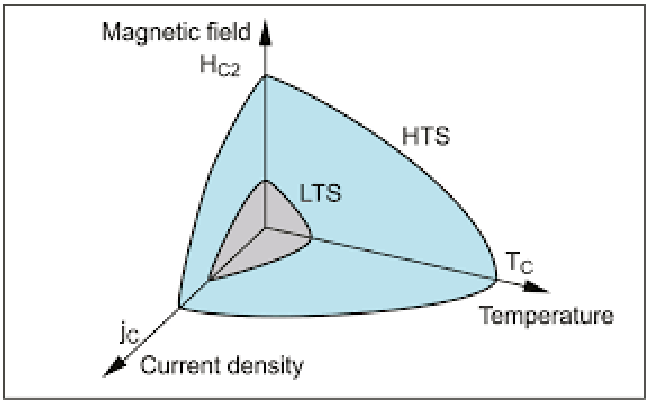

Figure 11. Superconductors' temperature-magnetic field-current density phase space

While superconductivity should be described in terms of quantum mechanical phenomena, this thesis concerns only with their application limits, described by the normal state transition, if any of the previous parameters exceeds a critical value. For a more understanding overview about superconductivity please refer to Appendix A. Conversely, if the material is in the so-called condensed electron state, it manifests truly zero electrical resistance for direct current.

As anticipated before, the three basic parameters on which evaluating a superconductor are the critical temperature, T_c, the critical magnetic field, B_c,and the critical current density, J_c. As it is clear from the figure above, a very big difference in terms of critical limits exists between Low Temperature Superconductors (LTS) and High Temperature Superconductors (HTS). For instance, T_c defines the maximum operating temperature and the robustness of the superconducting state against thermal energy. Much of the excitement and motivation toward applications of high temperature superconductivity was generated by the large number of materials with T_c exceeding the boiling point of liquid nitrogen (77 K), as shown in Figure 12. The possibility of reducing the use of helium, whose reserves are now running out and very expensive, makes HTS a revolutionary opportunity in the application of superconductivity.

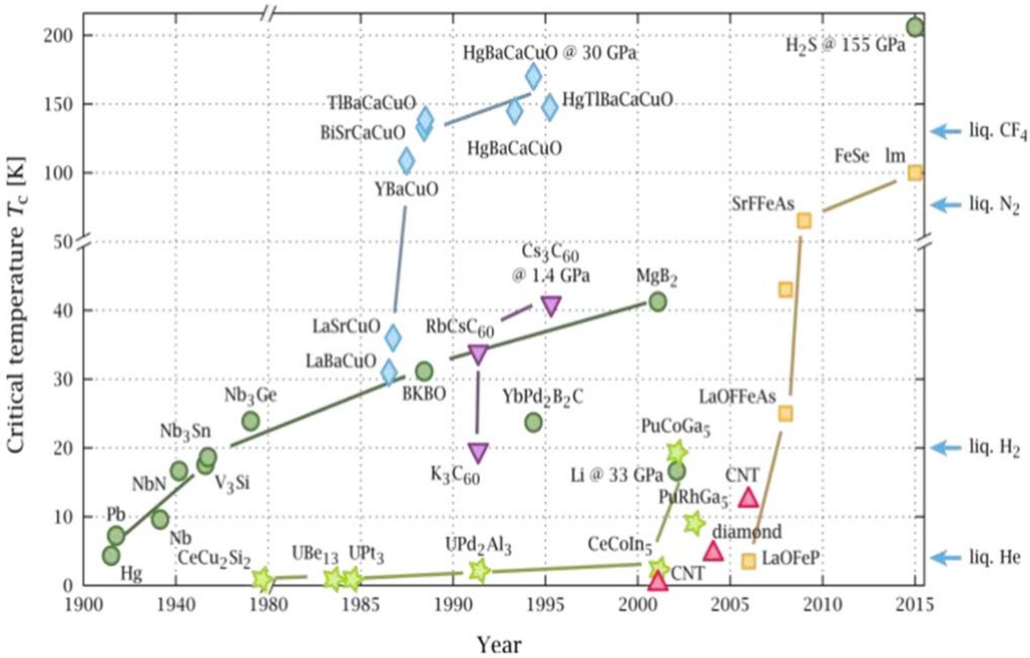

Figure 12. LTS vs HTS critical temperatures

Concerning the critical magnetic field, B_c, cuprates and some iron-based compounds have very high performances, while LTS and MgB_2 are in this sense a bit disadvantaged (see Figure 13). On the other hand, all the cuprate superconductors exhibit a high degree of anisotropy in fundamental physical properties including superconducting critical current and critical magnetic field.

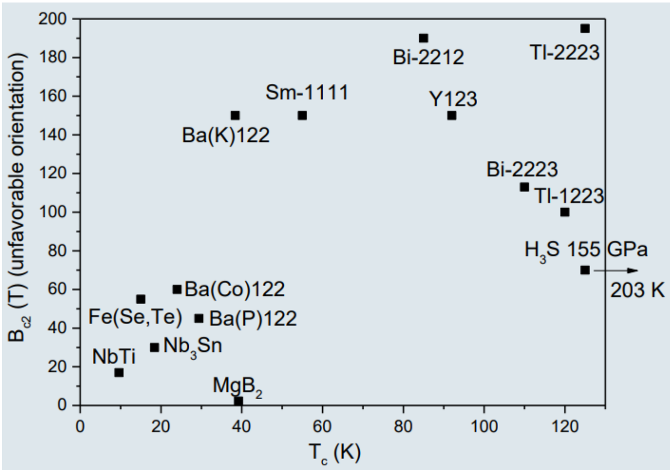

Figure 13. Critical magnetic field in the unfavorable direction versus critical temperature for various superconductors [4.3]

A serious consequence deals with the precipitous drop in J_c for mis-orientation angles greater than 2°. This means that proper manufacturing technique must be carefully considered to take advantage of the intrinsically high J_c of Type II superconductors. This parameter gives a clear overview on the maximum depinning critical current density over which the fixed magnetic flux lines within the superconductors starts to move due to the Lorentz forces.

Figure 14, Figure 15 and Figure 16 highlight this behavior for a REBCO-coated conductor at various temperatures [4.1-4.2]. While Figure 17 shows a comparison among different materials [4.3].

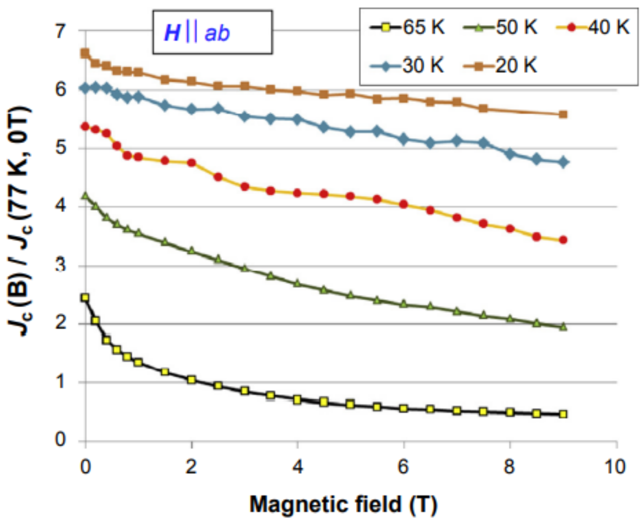

Figure 14. Normalized Jc vs H for applied magnetic field parallel to the ab plane at various temperatures [4.1]

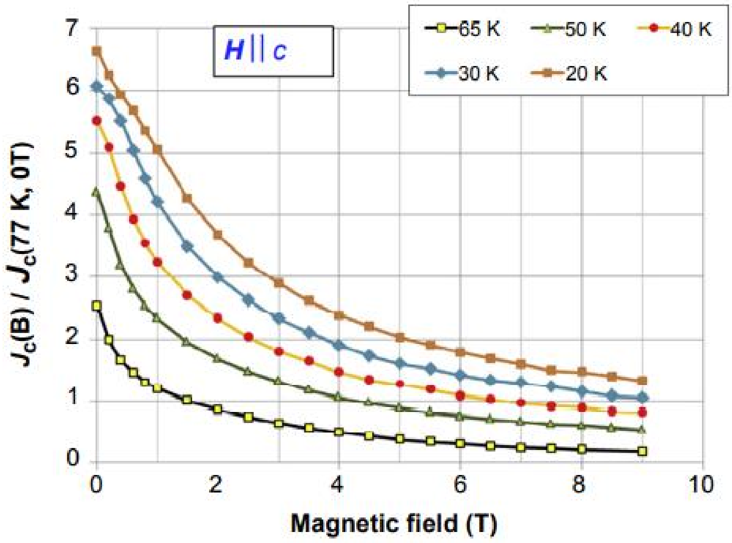

Figure 15. Normalized Jc vs H for applied magnetic field parallel to the c-axis at various temperatures [4.1]

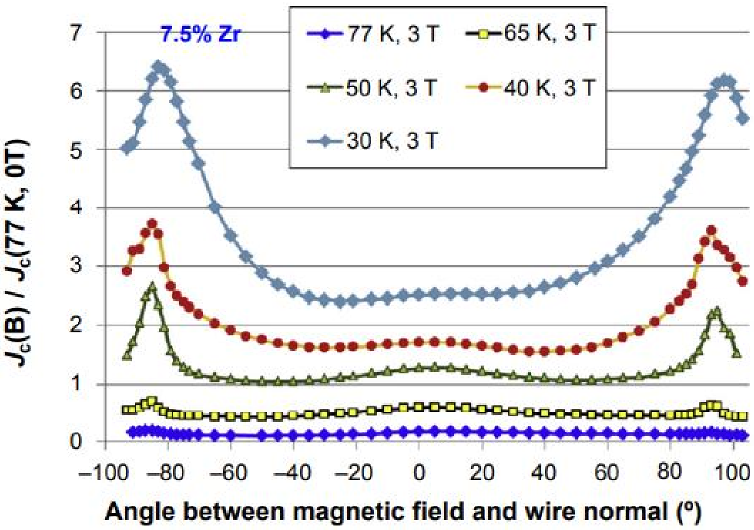

Figure 16. Normalized Jc vs angle between a 3 T applied magnetic field and a REBCO-CC tape at various temperatures [4.1]

As result, despite the large number of HTS materials discovered, for reasons coming down to performance and economics, only three practical HTS have been developed: Bi-2223 tapes, YBCO-coated conductor tapes, and Bi-2212 round wires.

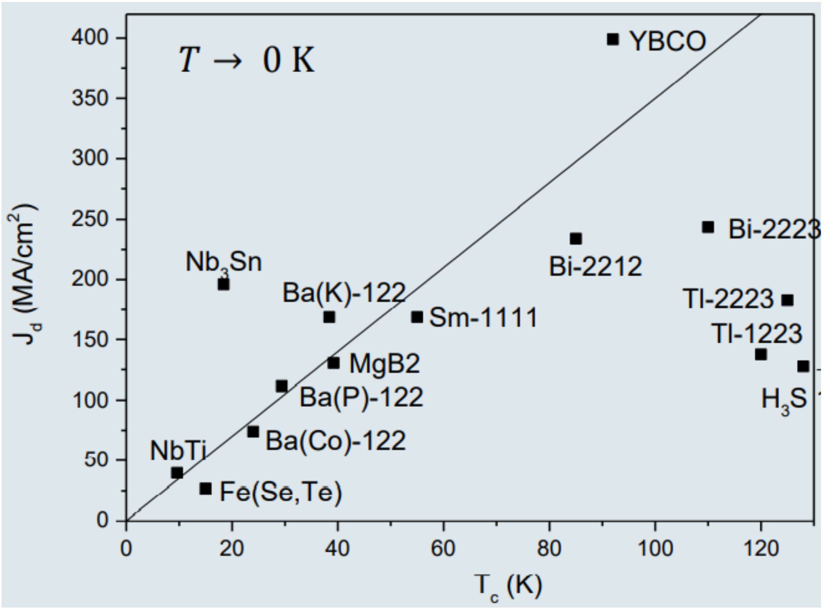

Figure 17. Critical current density versus critical temperature for various superconductors [4.3]

For this work, a second generation (2G) YBCO Coated Conductor (CC) tape manufactured by SuperPower® inc. has been adopted [4.4]. The choice was based on its ability to transport high current densities at high temperature and very high fields (up to 77 K and over 20 T, respectively). A cross section of a tape is reported, not to scale, in Figure 18.

The ampere-turn design here adopted is based on a stack of 7 commercial 12 mm-width 2G YBCO CC tapes, with a nominal current of more than 300 A at 77 K and self-field, so that conservatively a total effective current of 1 kA at 50 K can be retained for the stack. The high current safety margin takes care about the magnetic flux that perpendicularly overflows from the coil edges and strongly reduces the superconducting performance, as reported in Figure 16. Further analysis should consider the whole N-modules system, together with the increased current performances- thanks to the more efficiently trapped magnetic field lines- the lower stack length and the lower number of parallel tapes.

The choice of the 12 mm-width is the result of a gradient search optimization process- described in detail in the next paragraph- which brought to the highest inductance with the lowest stack length compared to other available products (4 mm-width, 6 mm-width) of the same factory. Table 2 summarizes the main specifications of the chosen tape.

Table 2. SCS12050 specifications

Manufacturer Model	Superpower Inc. SCS12050
Tape width (mm)	12
Tape thickness (mm)	0.1
YBCO layer thickness (μm)	1
Hastelloy layer thickness (μm)	50
Cu layer thickness (μm)	2 x 20
Critical current (self-field, 77 K) (A)	330
Minimum bending radius (mm)	5.5

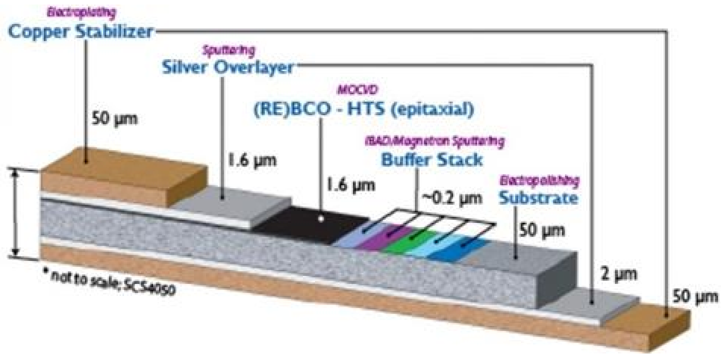

Figure 18. SCS4050 cross-section tape by SuperPower® Inc. [4.4]

4.1.2. Inductance maximization

Once the operating current is set, the inductance puts the limits on the system performance. A non-linear generalized reduced gradient (GRG) is used to maximize the self-inductance of the module with the lowest stack length, which is one of the most limiting factors in terms of cost. The objective function has been optimized respecting the following functional constraints: outer radius lower than 0.5m, inner radius higher than the minimum bending radius of the considered tape and a maximum magnetic field lower than 4 T.

This approach was carried out for three different tape-widths of the SCS (Surround Copper Stabilizer) group available at SuperPower® Inc.- which differ only in the transported critical current (100 A for 4 mm-with, 150 A for 6 mm-width, 300 for 12 mm-width at 77 K and self-field)- and for different cross-sectional layouts (square, rectangular) and mean radius of the windings.

The Wheeler's formulas, Equation (2), for a rectangular cross-section multi-layer air core solenoid, is adopted in the model [4.6].

$$L = \frac{0.8\left(a^2 N_{turn}^2 N_{layer}^2\right)}{6a + 9b + 10c} \tag{2}$$

While the Brooks' approximation, Equation (3), was adopted for the square cross-section, providing an optimal configuration when the mean radius is 3 times the dimension of the coil itself, or $2a = 3c$ [4.6].

$$L = 0.001 * a * N^2 * P_0'$$
$$P_0' = 4\pi\left[\frac{1}{2}\left\{1 + \frac{1}{6}\left(\frac{c}{2a}\right)^2\right\}\ln\frac{8}{\left(\frac{c}{2a}\right)^2} - 0.84834 + 0.2041\left(\frac{c}{2a}\right)^2\right] \tag{3}$$

Where (see Figure 19):

- a is the mean radius of windings (inch)
- b is the height of the coil (inch)
- c is the thickness of the coil (inch)

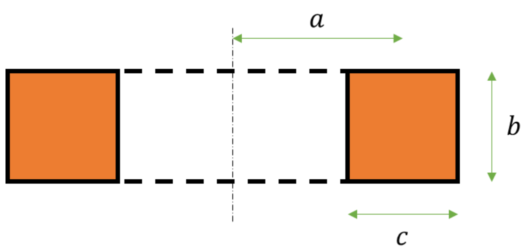

Figure 19. Cross-section sketch for the coil inductance calculation

For the winding pack of a single module, the optimized design points to a multi-layer coil with inner radius ~ 0.45 m, wound using 52 layers in parallel, each with 26 turns, with a total inductance of ~2 H and a maximum self-field below 4 T. Nine modules are needed for the entire SMES. The results of the optimization analysis are reported in Table 3.

Such design is checked and validated by a detailed 2D axisymmetric electro-magnetic model, purposely developed in COMSOL Multiphysics® [4.14].

Table 3. Design optimization results

Parameter	Value
Inner radius (cm)	44.6
Outer radius (cm)	48.3
Turns	26
Layers	52
Magnetic field (T)	4
Inductance (H)	2.1

4.1.3. Insulation

It must be considered that in many applications the parameters of the operating cycle (duration, charge, and discharge time, possibly idling) changes continuously and randomly [4.2].
Normal and abnormal switching of power electronics devices, thus, may generate transient over-voltages that take place in very short time compared to steady state, but that may have potential to damage any equipment that is subject to these transients, including the superconducting coil.
Therefore, it is essential to characterize the transients that may be experienced by the SMES coil and to carefully design a proper electrical insulation.
Independently of the shape of the magnet, the factor to be considered in the magnet insulation design are the turn-to-turn insulation, the layer-to-layer insulation, the magnet-to-cryocooler insulation and the magnet-to-ground insulation.
Among the various insulation techniques, a polyimide film wrapping has been adopted for the superconducting tapes. These films are widely used and differently from other materials provide a good trade-off between breakdown voltage and thermal properties.

Around each stack, 0.1 mm polyimide film is then used for electrical insulation. The latter was designed to withstand to a puncture breakdown of about 30 kV. The choice has been done considering 10 times off-normal over-voltage with respect the one that occurs during normal charging and discharging phase (~ 3 kV considering half-energy charge/discharge, with a cut-off frequency of 2 Hz).

Equation (4) is used to evaluate the minimum insulation thickness for charging/discharge half of the SMES magnetic energy ($\sim 0.5\ MJ$) with a cut-off frequency of 2 Hz. However, breaking down the coil into small pieces and analyzing the internal node voltages will give a better understanding of the transients that may affect the coil. A detailed modeling of the superconducting coil along with the power electronics interface modeling and control are essential in the electromagnetic transient interaction analysis.

$$\mathrm{V} = \mathrm{L}\frac{\mathrm{dI}}{\mathrm{dt}} \approx \mathrm{L}\frac{\Delta \mathrm{I}}{\Delta \mathrm{t}} = L\frac{\sqrt{\frac{2\Delta E}{L}}}{\frac{1}{f_{cut-off}}} \tag{4}$$

Here, L is the coil inductance (H), $\mathrm{dI/dt}$ *and* $\Delta\mathrm{I}/\Delta\mathrm{t}$ are respectively the differential and the macroscopic current rate (A/s), while ΔE *and* $f_{cut-off}$ are the energy variation and the cut-off frequency of charging/discharging (J and 1/s).

The entire module is then covered by 0.3 mm polyimide film for mechanical stability and magnet-to-cryostat/ground insulation. Figure 20 summarizes the basic design geometry of the SMES module.

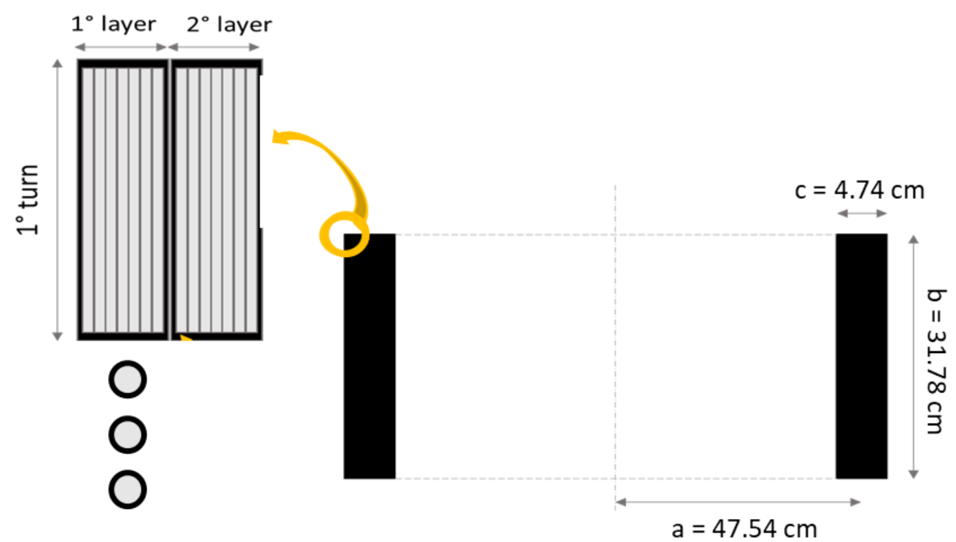

Figure 20. Basic designed coil sketch

4.2. Design validation

To validate the design a 2D axisymmetric FEM model has been built on COMSOL Multiphysics® [4.14]. The AC/DC module is used to describe the stationary electro-magnetic behavior of the present coil.

The problem of magneto-statics on a macroscopic level relies on the solution of the differential form of the Maxwell's equations (Equation (5)).

$$\begin{gathered} \nabla \times \boldsymbol{H} = \boldsymbol{J} \\ \mathbf{B} = \nabla \times \boldsymbol{A} \end{gathered} \tag{5}$$

Where:

- $\boldsymbol{H}$ is the magnetic field intensity (A/m)
- $\boldsymbol{J}$ is the current density (A)
- $\mathbf{B}$ is the magnetic flux density (T)
- $\boldsymbol{A}$ is the magnetic potential (J/A·m)

To obtain a close system, (6.a) (7.b) (8.c) includes constitutive relations that describe the macroscopic properties of the media (linear in the present).

$$\boldsymbol{J} = \sigma \boldsymbol{E} \tag{6.a}$$
$$\mathbf{B} = \mu_0 \mu_r \boldsymbol{H} \tag{7.b}$$
$$\mathbf{D} = \epsilon_0 \epsilon_r \boldsymbol{E} \tag{8.c}$$

Where:

- $\boldsymbol{E}$ is the electric field intensity (V/m)
- $\mathbf{D}$ is the electric displacement (C·m^2)
- $\sigma, \mu_0, \mu_r, \epsilon_0, \epsilon_r$ are respectively the electrical conductivity (S/m), the permeability of vacuum and the relative one (H/m), the permittivity of vacuum and the relative one (F/m).

Finally, to get a full description of an electromagnetics problem, boundary conditions must be specified at material interfaces and physical boundaries and initial condition mut be specified everywhere. In the present case, an infinite air domain has been considered at which magnetic insulation can be applied:

$$\mathbf{n} \times \mathbf{A} = 0 \tag{7.a}$$
$$\mathbf{A_0} = 0 \tag{7.b}$$

While a null magnetic vector potential can be used as initial guess for the present non-linear problem.

The magnetic field within all domains but the SC stacks is described by the Ampere law. The stacks are modelled as normal conductors (linear constitutive relation with 'infinite' electrical conductivity) transporting a uniform current of 1050 A. The reason for neglecting the complex superconducting behavior of the coil relies on the interest in evaluating the maximum external magnetic field, overshadowing the actual non-uniform current density and the corresponding magnetic flux within the coil itself. This choice is not a limitation but a simplification of the problem, which allows to speed up the model and get acceptable results.
Figure 21 shows the magnetic flux density distribution around the coil while Figure 22 shows the norm of the magnetic flux along the central line and on the top line of the coil, respectively.

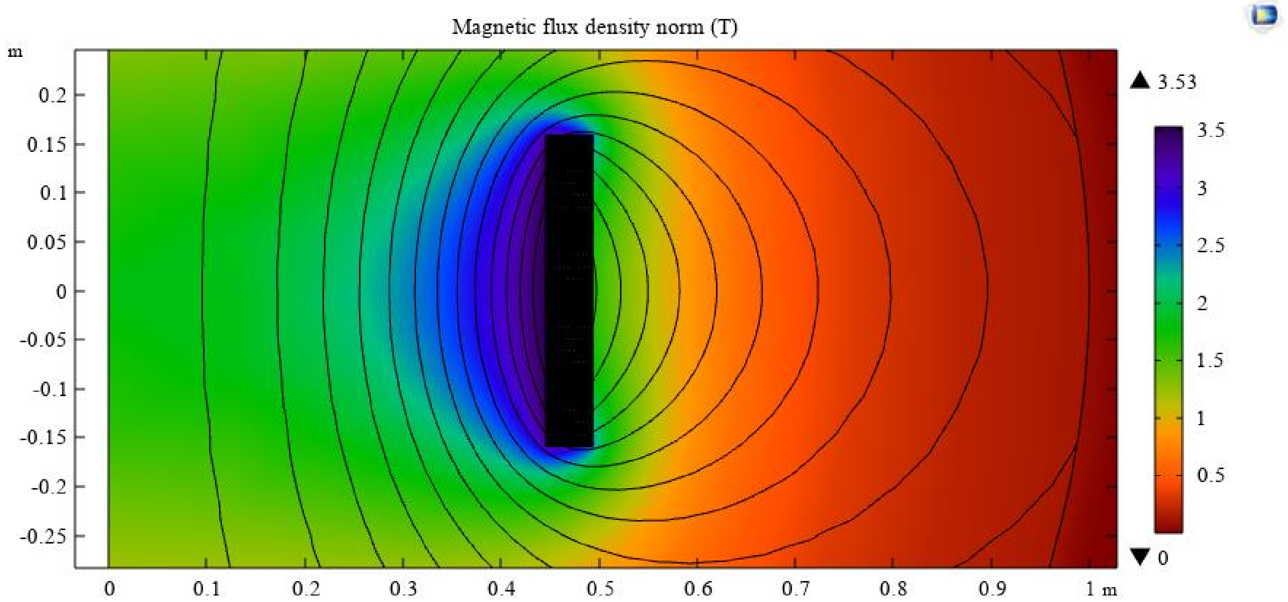

Figure 21. Magnetic flux density norm

The maximum magnetic flux density is at the center of the inner part of the magnet, as expected, and its value is lower than the chosen constraint (4 T); while the computed inductance is about 2 H (very close to the one calculated with the Wheeler's approximation).
Of course, the more sophisticated equations implemented in COMSOL Multiphysics with respect the one used in the analytical optimization have led to slightly different results; however, a second difference between the two models has been deliberately introduced due to the geometry itself: while the optimization analysis did not care about the electrical insulation, in the computational model the polyimide film thickness is added for evaluating how much the results would have been engraved.
Note that despite the maximum magnetic field arises at the center of the coil inner radius, its value on the top/bottom (orange circle in Figure 22) is still quite high and it is perpendicularly directed towards the coil itself. This means that due to the strong anisotropy of the YBCO tapes, the inner top and bottom part on the coil would be the most affected in case of unwanted abnormal conditions, and that of major interest during transients.

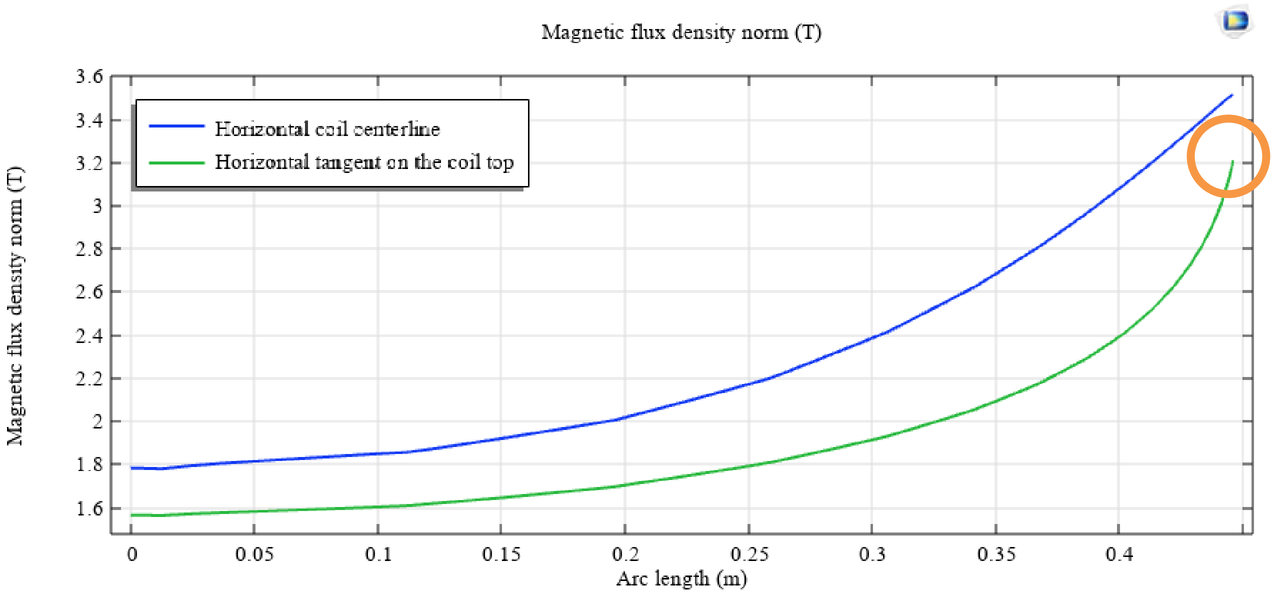

Figure 22. Magnetic flux density norm along the central line (blue) and on the top line (green) of the coil

4.3. References

[4.1] C. Rey, “Superconductors in the Power Grid: Materials and Applications”, Woodhead Publishing Series in Energy: No. 65.

[4.2] Z. Melhem, “High temperature superconductors (HTS) for energy applications”, Woodhead Publishing Series in Energy, No. 27.

[4.3] M. Eisterer, “HTS versus LTS: physics, technology, and application prospects”, EUCA2017, Geneva, 2017.

[4.4] SuperPower Inc., A Furukawa Company, Available: https://www.superpower-inc.com.

[4.5] Y. Iwasa, “Case studies in superconducting magnets: design and operational issues”, Second Edition, Springer, ISBN 978-0-387-09799-2.

[4.6] H. B. Brooks, “Design of standards of inductance, and the proposed use of model reactors in the design of air- core and iron-core reactors”, Bureau of Standards Journal of Research, Vol. 7.

[4.7] A. Morandi, M. Fabbri, B. Gholizad, F. Grilli, F. Sirois, V. M. R. Zermeño, “Design and Comparison of a 1-MW/5-s HTS SMES With Toroidal and Solenoidal Geometry, IEEE Trans. Applied Supercond., Vol. 26, No. 4, June 2016.

[4.8] A. Morandi, B. Gholizad, M. Fabbri, “Design and performance of a 1MW-5s high temperature superconductor magnetic energy storage system”, Supercond. Sci. Technol. 29 (2016) 015014 (12pp).

[4.9] A. W. Zimmermann, S. M. Sharkh, “Design of a 1 MJ/100 kW high temperature superconducting magnet for energy storage”, Energy Reports, Vol. 6, pp. 180–188, 2020.

[4.10] U. Bhunia, J. Akhter, C. Nandi, G. Pal, S. Saha, “Design of a 4.5 MJ/1 MW sectored toroidal superconducting energy storage magnet”, Cryogenics, Vol. 63, pp. 186–198, 2014.

[4.11] Y. Li, P. Song, Y. Kang, F. Feng, T. Qu, “Design of a 30-K/4-kJ HTS magnet cryocooled with solid nitrogen”, IEEE Trans. Applied Supercond., Vol. 28, No. 4, June 2018.

[4.12] M. A. Al Zaman, M.R. Islam, H.M.A.R. Maruf, “Study on conceptual designs of superconducting coil for energy storage in SMES”, Journal of Physics, Vol. 1, pp. 111-120, 2020.

[4.13] K. Shikimachi, N. Hirano, S. Nagaya, H. Kawashima, K. Higashikawa, T. Nakamura, “System coordination of 2 GJ class YBCO SMES for power system control, IEEE Trans. Applied Supercond., Vol. 19, No. 3, June 2009.

[4.14] COMSOL Multiphysics® v. 5.4., COMSOL AB, Stockholm, Sweden. Available: https://www.comsol.com.

[4.15] J. H. Choi, H. G. Cheon, J. W. Choi, H. J. Kim, K. C. Seong, S. H. Kim, “A study on basic insulation characteristics of 2.5 MJ class conduction-cooled HTS SMES”, IEEE Trans. on Applied Supercond., Vol. 20, No. 3, June 2010.

[4.16] J. H. Choi, D. S. Kwag, H. G. Cheon, H. J. Kim, K. C. Seong, S. H. Kim, “The insulation characteristics of coil—cryocooler for conduction cooled HTS SMES”, IEEE Trans. on Applied Supercond., Vol. 17, No. 2, June 2007.

Politecnico
di Torino
1859

5. CRYOSTAT DESIGN

The cryostat design is aimed to maintain the system at cryogenic temperature, to guarantee easy access to internal component, to reduce vibration and guarantee alignment of the equipment therein, to ensure the electro-magnetic screening, and to guarantee the safety and the integrity requirements. This means that it is not just a matter of temperatures, but it is important to put cryogenics in perspective, including material selection, design of the thermal insulation system, cost, complexity, and size [5.1].

The starting point for a cryostat design relies on the identification of the static and dynamic heat loads that enter the system. The main ones can be summarized as follow:

1) Radiation between the cryostat's walls
2) Convection in the evacuated space between the cryostat's walls
3) Conduction through the magnet support and cryostat structural elements
4) Combination of conduction and Joule dissipation of current leads
5) Dissipation within the magnet.

Different configuration and cooling techniques have been studied and adopted during years to face all these requirements [5.2]. These can be grouped in three main categories: the bath-cooled and the force-cooled method, which are part of the "wet" configurations, and the cryocooled (even called conduction-cooled), which is part of the "dry" configurations [4.5].

The choice of one method than another is based on a trade-off evaluation among the following points:

- Availability/Reliability/Maintenance
- Complexity/Intrusiveness
- Performance/Cost (utility requirements, depletion of cryogen reserves, …)
- Cool-down time and magnet cryo-stability.

The key role of the present work is to minimize the intrusiveness of the system and to maximize its availability, reliability, and maintainability. In this perspective a dry, cryogen-free, cooling system has been chosen and analysed, considering different cryocooling options, the minimum number of cryocoolers for maintaining the operating temperatures, the thermal behaviour of materials, and the thermal stability of the SC magnet. Indeed, a cryogen-free cooling system is not only less cumbersome to operate and maintain but eliminates the pipes

required to circulate the cryogen and its containment structure too. As results, it also eliminates the possibility of over-pressurization of the cryostat due to accidental scenarios.
This choice was achievable because of the peculiar characteristics of the chosen tape (i.e., extremely thin superconducting layer parallel to the magnetic field, very high ‘n’ value, …) and the toroidal geometry of the system which minimize Joule losses. As a result, it was possible to reduce the required cryo-cooling capacity and use simpler configurations.

5.1. Methodology

An AISI 304 SS vacuum vessel delimits the cryostat from the environment. For reducing the radiation between the cryostat walls, very low emissive materials are used, and an actively cooled radiation shield (Aluminized polyimide film MLI) is added between the high temperature and the low temperature surfaces. A low conductivity thermal shield (Aluminum 6061-T6) is placed between the outermost cryostat wall and the coil to intercept the heat at an intermediate temperature and reduce the conduction heat leak to the lowest temperature.
As result, a two-stages cryogen-free refrigeration can be adopted: the cryostat thermal insulation and the current leads are cooled at the first warmer stage (~ 77 K) while the magnet itself is cooled at the colder second stage (~ 50 K). The thermal link between the two-stages and the refrigeration system is provided by two copper plates. This connection between cold heads and thermal loads can also be made ‘indirect’ using conducting flexible wires to reduce the vibration propagation of the cryocooler through the system.
Despite the very low thermal inertia (i.e., absence of a cryogenic bath), fast charging and discharging can be safely established (but at the price of longer recovery time).
Nevertheless, there are necessary some mechanical junctions between the room temperature structure and the coil in order to support it. These junctions are generally tie rods made of stainless steel, glass fiber reinforced plastic or carbon fiber reinforced plastic, i.e., materials with high mechanical resistance but low thermal conductivity.
Other sources of heating are, unavoidably, the current leads and the AC losses (eddy currents, magnetization losses, coupling losses, magnetic losses, …) regarding the magnet itself.
The basic cryostat design parameters are listed in Table 4, following a similar design as in [5.3].

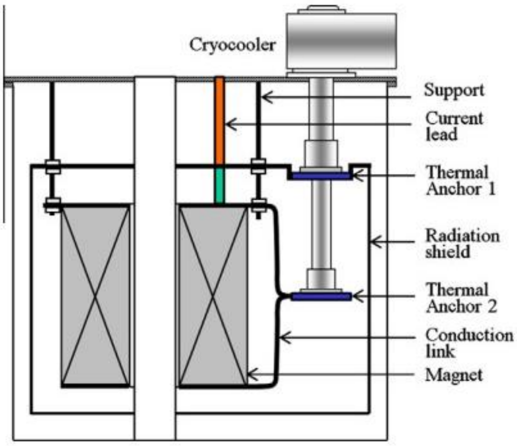

Figure 23. Basic cryostat design as in [5.3]

Table 4. Cryostat design parameters

Component	Parameter	Value
Vacuum Vessel (VV)	Outer radius (m)	0.8
	Thickness (mm)	5
	Height (m)	0.8
Thermal Shield (TS)	Outer radius (m)	0.7
	Thickness (mm)	3
	Height (m)	0.6
Radiation Shield (RS)	Layers	30
	Thickness (mm)	0.9
	Height (m)	0.6

5.1.1. Cryocooler

To provide the necessary refrigeration power for reaching cryogenic temperatures, a 4 K Gifford-McMahon cryocooler regenerative heat exchanger SRDK-415D is identified, with the characteristic and cooling capacity reported in [5.4].

The basic components of any GM cryocooler are as listed below and reported in Figure 24:

- Helium compressor – scroll/reciprocating type.
- Flex lines – HP line, LP line.
- Regenerator(s) and Displacer(s).
- Valve mechanism – rotary, solenoid, poppet.
- Cooling arrangements – Air or water cooled

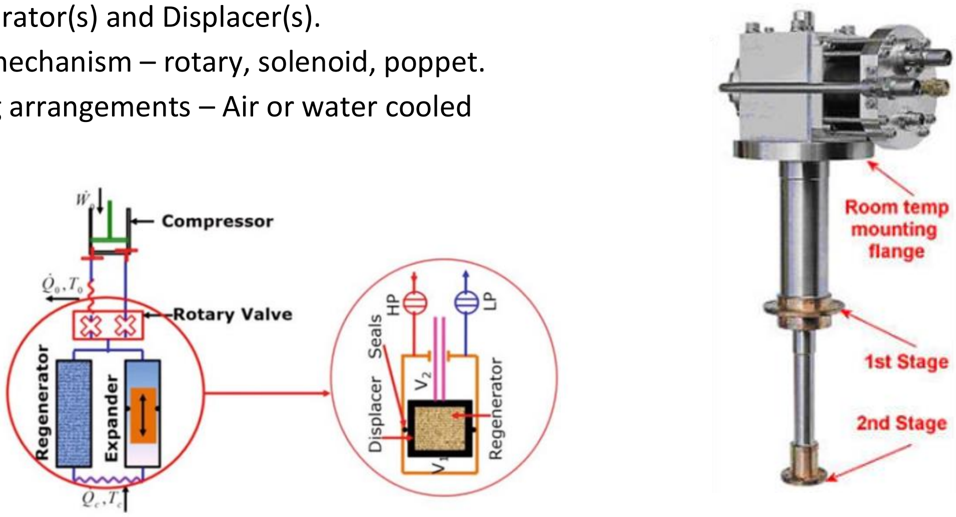

Figure 24. Schematic and technical diagram of G-M cryocooler

From a practical point of view, GM cryocoolers **are highly reliable**. The rotary valve facilitates the *production of any kind of pressure*-wave as per the requirement of system. The presence of the valve mechanism also *allows the cold head to be placed at a distance from the compressor and connected by flexible lines* for the high- and low-pressure gas. Losing some cooling power, the GM *can operate in any orientation without affecting the base temperature* and, in general, are quite cheap.

The main drawbacks are conversely a very low efficiency (about 25 %) and a strong vibration due to the displacer motion, which easily propagate within the cryostat [5.5].

5.2. Design validation

A 2D axisymmetric geometry is adopted to model the cryostat and the coil to solve the conduction equation and compute the temperature field distribution, the required cooling power, and cool down time.

The heat transfer module of COMSOL Multiphysics® solves the following Equation (8):

$$\rho C_p \frac{\partial T}{\partial t} + \nabla \cdot (\boldsymbol{q} + \boldsymbol{q_r}) = Q \tag{8}$$

Where:

- ρ is de density (kg/m^3)
- C_p is the specific heat capacity (J/kg·K)
- T is the absolute temperature (K)
- $\boldsymbol{q}$ is the heat flux by conduction (W/m^2)
- $\boldsymbol{q_r}$ is the heat flux by radiation (W/m^2)
- Q contains additional heat source/sink (W/m^3)

Equation (8) considers the heat transfer by radiation as an additional source term to the more general heat equation. This source accounts for the difference between incident radiation, or *irradiation*, G -that stands for the mutual irradiation coming from other boundaries being considered neither external radiation sources nor ambient irradiation- and radiation leaving the surface, or *radiosity*, J:

$$q_r = (1 - \rho_s)G - J \tag{9}$$

By itself, the *radiosity* (Equation (10)) is the sum of diffusely reflected and emitted radiation. Being our system composed by diffuse-gray surfaces, J can be defined by:

$$J = \rho_d G + \varepsilon e_b(T) \tag{10}$$

Here:

- ε is the surface emissivity independent of the radiation wavelength
- $e_b(T)$ is the black-body hemispherical total emissive power

The whole stack was considered as a single element, taking into account the material properties of each layer that composes the tape, including the buffer layer. The thermal properties, mainly the thermal conductivity and the specific heat, are introduced in the FEM model as function of temperature. The density, reported in Table 5, and the emissivity values are instead taken constant with temperature. Figure 25 and Figure 26 report the thermal conductivity and the specific heat for all the materials considered, while the numerical values are reported in Appendix A.

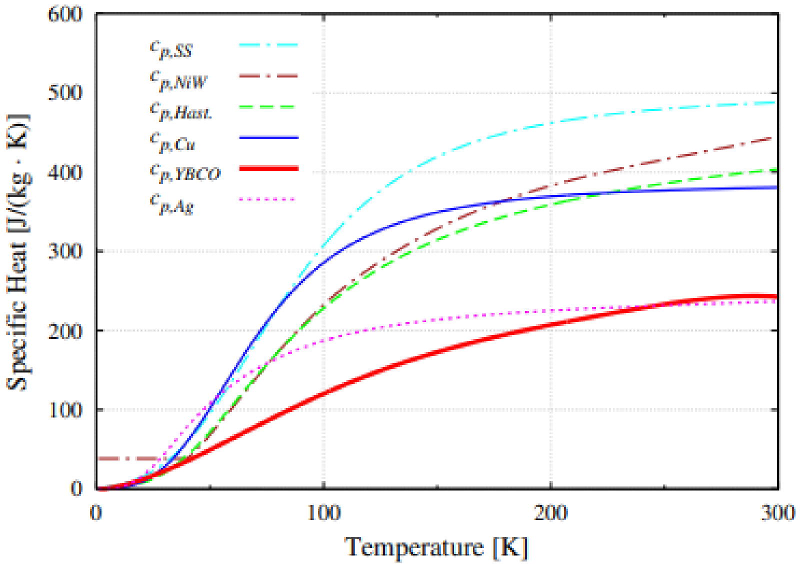

Figure 25. Specific heat as a function of temperature of the material composing the YBCO tapes

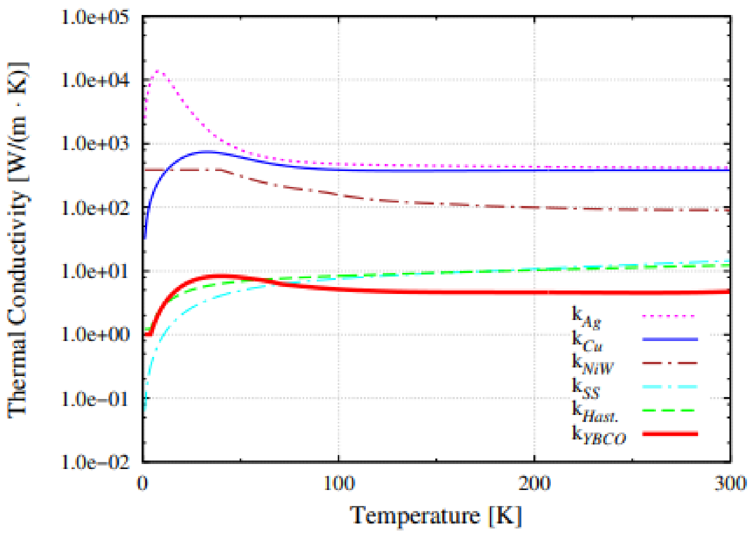

Figure 26. Thermal conductivity as a function of temperature of the material composing the YBCO tapes

The anisotropic nature of the HTS is also considered, evaluating homogenized properties in the axial/poloidal and the radial direction by means of a resistive electrical analogy.

Figure 27 (a) and (b) highlights this point and shows the equations respectively implemented, exactly as in [5.6].

Table 5. Material densities

Material	$\rho \left[\frac{kg}{m^3}\right]$
Cu	8960
Ag	10630
Hastelloy(R)	8890
YBCO	6380
Stainless Steel	7900
NiW	10400

On the other hand, in this first simple model, current leads and coil supports are not considered being not well representable by a 2D axisymmetric configuration. As results, part of the heat load (due to heat conduction through the solid materials) coming from the environment is not accounted for.

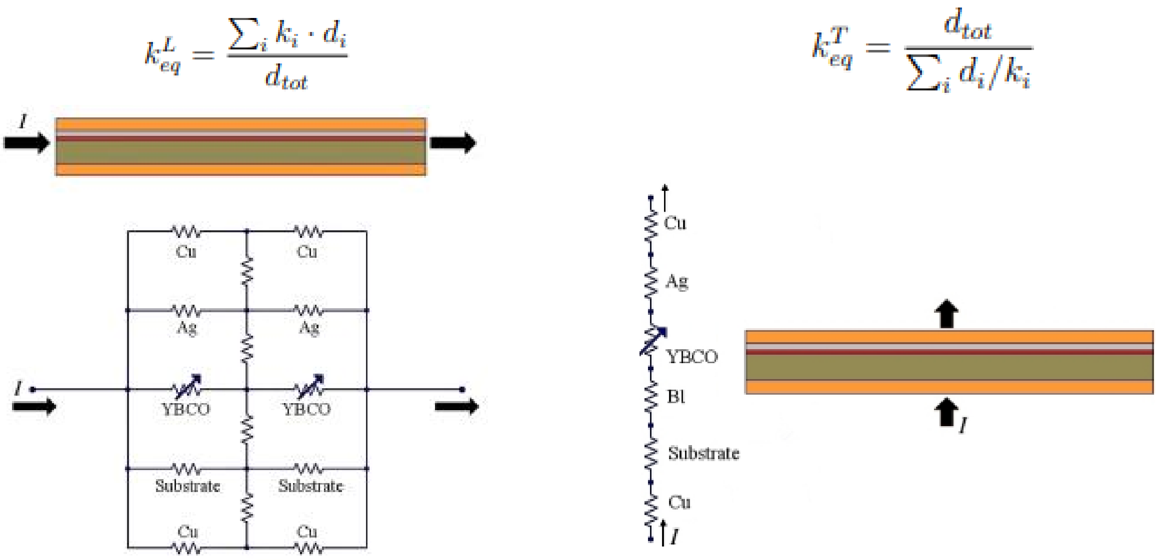

Figure 27. Sketch of the resistance equivalent circuit in case of longitudinal flow (a) and transversal flow (b), respectively [5.6].

Despite this simplification, as will be clarified in the following results, the cooling capacity of the cryocooler is still far larger that the power required to assess the radiation load. Meaning that these non-accounted thermal loads can be also faced by the same cryocooler.
A stationary study has been performed fixing the operating temperature at the two cryocooler thermal interfaces- represented in Figure 28 as section 5a and 5b, respectively- for evaluating the cooling requirements and the number of cryocoolers needed to satisfy the specifications.

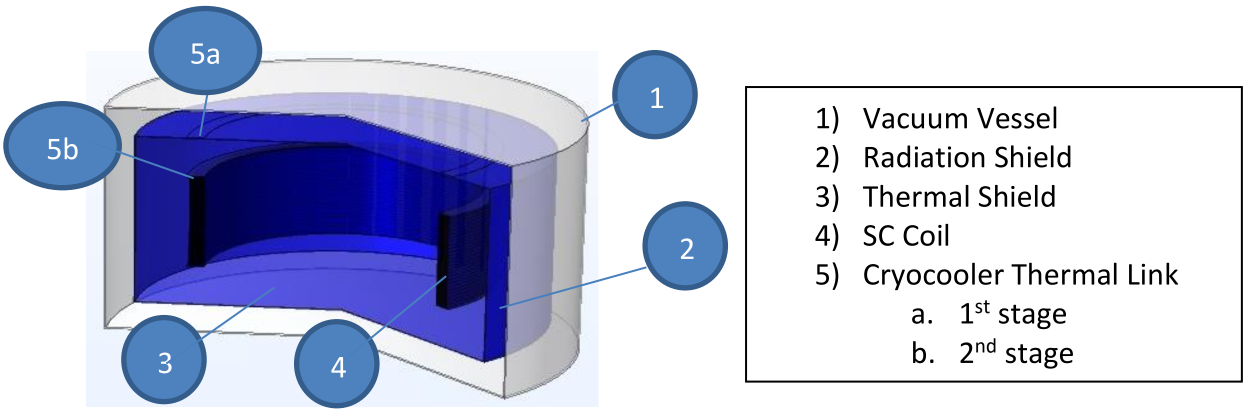

Figure 28. Cryostat sketch built for the design validation

The result shows that, because of the very high cooling capacity of the SRDK-415D at the rated temperature, one single cryocooler would be sufficient to cool down the system, and safely keep it at 77 K for 1st stage and 50 K for the 2nd stage in absence of any loss but radiation. The required power capacities are indeed 13.2 W and 0.1 W, respectively. In steady state condition, the temperature gradient within the entire magnets is also extremely small (about 0.01 K).

A second time-dependent study has then been solved substituting the fixed temperature at the two cryocooler thermal interfaces with the cooling capacity of the cryocooler itself, respectively at the first and the second stage. Aim of this second study is the evaluation of the cool down time of the system, that lasts for 250 hours and takes the values each 5 minutes. As shown in Figure 29, while the thermal shield gets the operating temperature in about 70 hours, the coil requires up to 170 hours to reach 50 K.

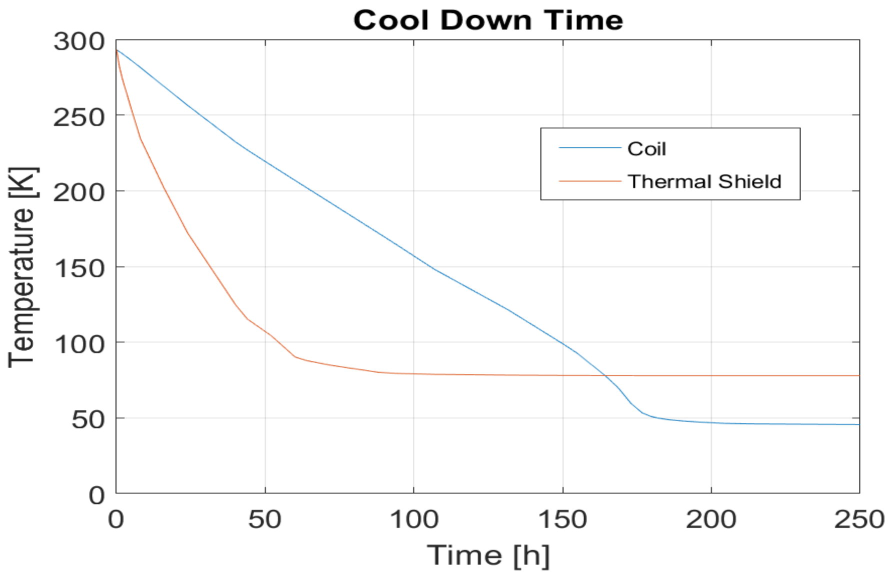

Figure 29. Cryostat cool down time

It is clear that about one week cooling time is quite high and should be reduced as much as feasibly possible optimizing dimensions and geometry of the cryostat itself. However, since the main challenging component is the SCM, may a change in the cooling technique (i.e., “wet” cooling approach) will be necessary.

5.3. References

[5.1] S. W. Van Sciver, J. Sangkwon "Cryostat design case studies, principles and engineering", J.G. Weisend, II Editor.

[5.2] Jung-Bin Song, Haigun Lee. Mixed cryogen cooling systems for HTS power applications: A status report of progress in Korea University. Cryogenics 52 (2012) 648–655.

[5.3] Y. S. Choi, D. L. Kim, D. W. Shin, "Optimal cool-down time of a 4 K superconducting magnet cooled by a two-stage cryocooler", Cryogenics, Vol. 52, pp. 13–18, 2012.

[5.4] Ho-Myung Chang, Y.S. Choi, S. W. Van Sciver, "Optimization of operating temperature in cryocooled HTS magnets for compactness and efficiency", Cryogenics, Vol. 42, pp. 787–794, 2002.

[5.5] T. Wirths et al., "Load map of Sumitomo 415DP cryocooler in the temperature range of 40-400K", IOP Conf. Ser.: Mater. Sci. Eng. 755 012042, 2020.

[5.5] M. D. Atrey, "Cryocoolers Theory and Applications", International Cryogenics Monograph Series Series Editors: J. G. Weisend II · Sangkwon Jeong

[5.6] M. Casali, "Experimental analysis and numerical simulation of quench in superconducting HTS tapes and coils", Ph.D. thesis, 2014.

[5.7] K. Shikimachi, N. Hirano, S. Nagaya, H. Kawashima, K. Higashikawa, T. Nakamura, "System coordination of 2 GJ class YBCO SMES for power system control", IEEE Trans. on Applied Supercond., Vol. 19, No. 3, June 2009.

Politecnico di Torino

6. POWER FEEDING SYSTEM

To guarantee the electrical connection to the grid a system of current leads must be foreseen. This is commonly divided in two parts: the ambient temperature current leads, located outside the cryostat, and the cryogenic current leads, located inside the cryostat. The design of the cable at ambient temperature is quite standard, the only requirements are a suitable cross-section to carrying the rated current, without an excessive overheating, and a proper insulation. The section within the cryostat must instead carefully designed: a normal cryogenic conductor, between the SS chamber and the 1^{st} stage, is commonly used to minimize the cost and to make it properly work (the temperature is still too high for using SC cables); while superconducting current leads (usually made of BSCCO or YBCO tapes) are adopted between the 1^{st} and the 2^{nd} stage to reduce at most the joule losses.

6.1. References

[6.1] M. Casali, "Experimental analysis and numerical simulation of quench in superconducting HTS tapes and coils", Ph. D. Thesis, 2014.

[6.2] R. Heller ∗, W.H. Fietz, A. Kienzler, "High power high temperature superconductor current leads at KIT", Fusion Engineering and Design, Vol. 125, pp. 294–298, 2017.

[6.3] P. Bauer, "Development of HTS Current Leads for the ITER Project", ITR-18-001, 2018.

[6.4] A. Ballarino, "Current Leads, Links and Buses", CERN, Geneva, Switzerland.

Politecnico di Torino

7. CONCLUSION AND PERSPECTIVES

A Functional Analysis and Allocation approach has been applied here for designing a complex SMES system. Throughout this approach all the sub-system and components of a SMES has been broken down and some of them designed in terms of their own independent functions and constraints.

Commercially available high temperature superconductor (HTS) YBCO tapes have been considered for the design of the magnet. Also, the cooling power requirement for this case and the cool down time of the SMES system has been evaluated.

Using HTS and less complex cryostats allows to design more and more efficient SMES, to be used for the present and crucial energy transition towards a cleaner world.

To further assess the soundness of the design, more comprehensive 3D and multi-physics simulations are needed to fully understand the material behaviour (i.e., thermo-mechanics analysis, thermo-magnetic analysis, …), and more sophisticated modelling should include and implement the superconducting behaviour of the coil.

A cryostat optimization must be performed to reduce the cool down time as much as possible, and a multi-elemental toroidal SMES design should be investigated. While a final cost-performance analysis could be an interesting conclusion to understand which improvement will definitely lead these architectures to a more spread commercialisation.

Appendix A

A.1. Superconductivity

The story of superconductivity begins in 1911 when *Kamerlingh Onnes*, while studying the resistivity of pure metals, notice that below 4.2 K the resistance of a mercury sample suddenly dropped. As in many other metals, the resistance of mercury decreased steadily upon cooling, but dropped suddenly at 4.2 K, and became undetectably small (see Figure 30).

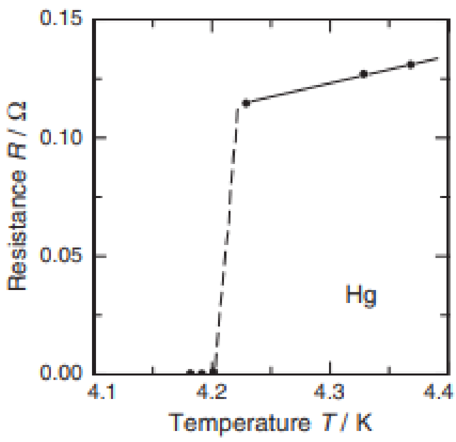

Figure 30. Historical data on the temperature dependence of the electrical resistance of a thread of mercury

Later experiments proved that while passing through the superconducting state the resistance was not only very small, but in fact zero, and that different materials had different transition temperatures.

In 1933, *Meissner* and *Ochsenfeld* discovered that superconductors are not only characterized by the absence of resistance but also by their *ideal diamagnetism. During their experiment they observed that, differently from what happened in 'ideal conductors',* the expulsion of the magnetic flux from the superconductors- as reported in Figure 31- was always verified: the *Meissner effect*.

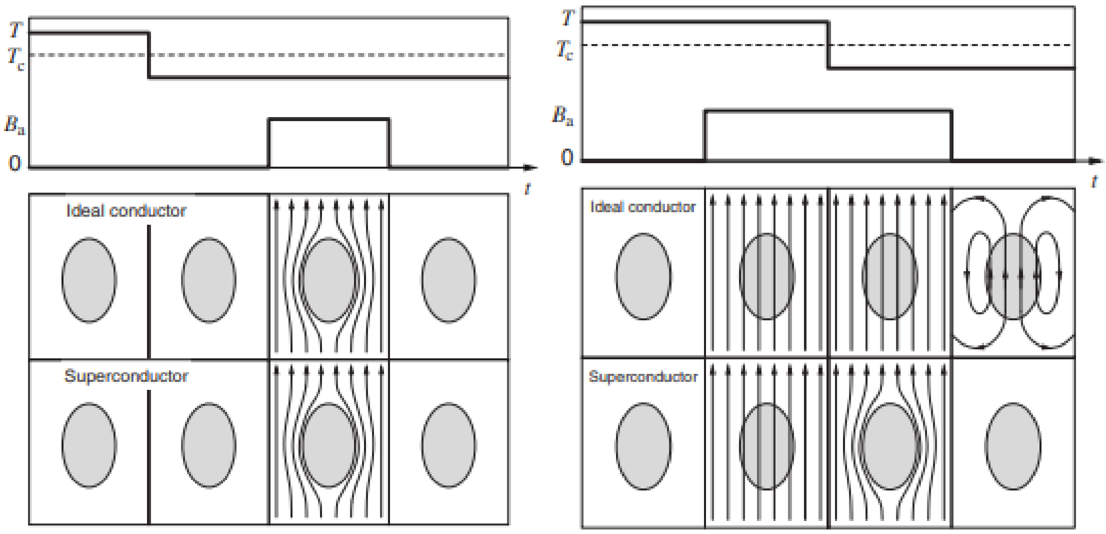

Figure 31. 'Ideal conductor' and superconductor in a magnetic field

However, this ideal diamagnetism was observed to be present only for applied magnetic field lower than the temperature dependent threshold limits called *critical magnetic fields*. As shown in Figure 32 if the external field is increased, screening breaks down at the critical magnetic field B_c, and a transition to the normal state takes place.

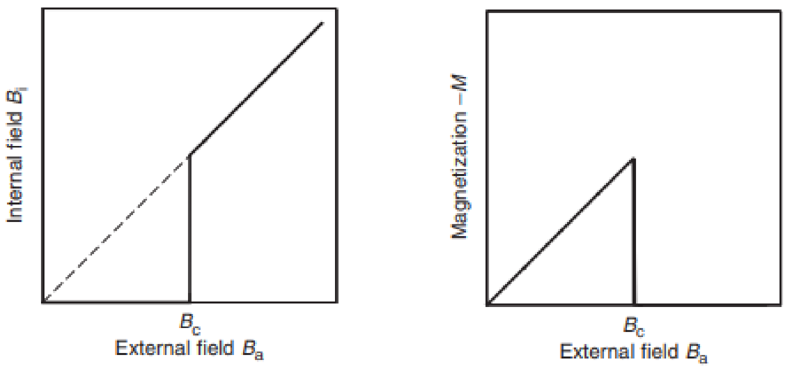

Figure 32. (a) Magnetic field inside a type I superconductor, and (b) its (negative) magnetization as a function of the applied magnetic field

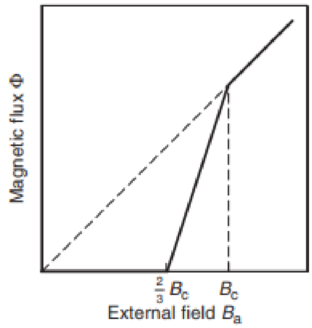

Figure 33. Magnetic flux through the equatorial plane of a superconducting sphere as a function of external field

Furthermore, the shape of the specimen has an important influence on the magnetic behavior of superconductors. In fact, with different shapes, the magnetization alters the magnetic field seen by the specimen, resulting into a state of alternating regions of superconducting and normal material- parallel oriented to the applied field- called *intermediate state* (Figure 33).

Three years later, *Lev Shubnikov* and his colleagues in Kharkov observed a new type of superconducting behavior in high-quality metal alloy samples. But only more than 20 years later *Ginzburg, Landau*, and *Gorkov*, were able to give an explanation for the existence of two types of superconductors. In these materials, such as transition metals, metallic glasses, and the novel high-T_c superconductors, appears a new phase, called *mixed state* or *Shubnikov phase,* in which the magnetic flux is allowed to penetrate in the form of thin filaments (*flux vortices*) within normal conducting islands (Figure 34).

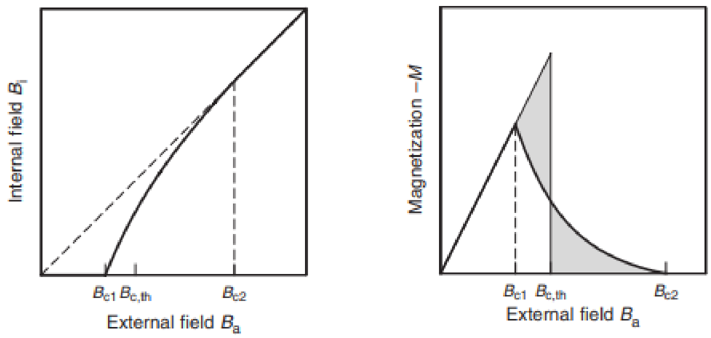

Figure 34. (a) Internal field in a type II superconductor, and (b) its (negative) magnetization as a function of the applied magnetic field.

In the mixed state, these flux vortices enter as quantized fluxons and are pinned by grain boundaries and crystal defects. Defects, or in general local depressions of the order parameter $|\psi|^2$, hinders vortex motion and still brings to (nearly) zero the dissipation. The fluxons can be however put in motion because of thermal activation (flux creep) and because of Lorentz force if the *depinning* critical current density, J_c, is reached and overcome. This phenomenon gives rise to an electromotive force that determines a net dissipation in the superconductor, as shown in Figure 35.

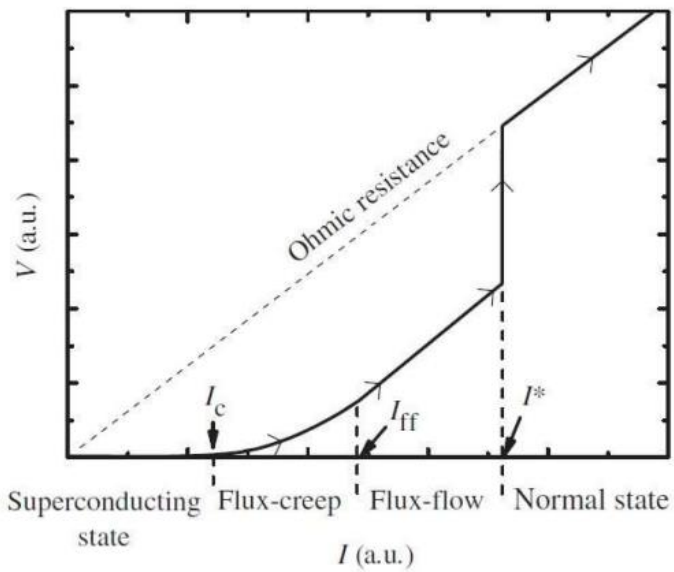

Figure 35. Net dissipation in a type II superconductor due to the electromotive force

As result, higher is the transport current higher is the vortex instability; if the electromotive dissipation established a thermal runaway (quench), the superconductor abruptly passes to the normal state and the vortex avalanches can locally damage it. This condition sets an upper bound to the rate of magnetic field sweeping and/or to the applied current, depending on the material, its geometry and also the (cryogenic) environment. However, the upper critical field B_{c2} of type II superconductors may be several hundred times larger than the critical field B_c of type I superconductors, and this is the reason why, despite the non-perfect diamagnetism, type II superconductors are today the most used one.

Politecnico di Torino

A.2. References

[A.1] Francesco Laviano, “Superconductors: introduction to superconductivity and superconducting materials”, notes.

[A.2] Christian Enss, Siegfried Hunklinger , “Low-Temperature Physics”, Springer-Verlag Berlin Heidelberg 2005.

Appendix B

B.1. Thermal Properties of 2G YBCO-CC

Table 6. Specific heat of the tape's materials at various temperatures

T [K]	$c_{p,Cu}$	$c_{p,Ag}$	$c_{p,Hast}$	$c_{p,YBCO}$	$c_{p,NiW}$	$c_{p,SS}$
5	0.192	0.232	0.740	0.667	38.180	2.481
10	1.206	1.798	1.929	3.470	38.180	5.489
15	3.839	6.844	4.017	7.182	38.180	9.545
20	8.814	15.675	7.452	11.678	38.180	15.128
25	16.706	28.521	12.684	16.845	38.180	22.645
30	27.860	44.477	20.163	22.575	38.180	32.404
35	42.327	61.540	30.337	28.772	38.180	44.590
40	59.843	78.557	43.656	35.345	38.180	59.238
45	79.863	94.071	56.207	42.211	52.277	76.231
50	101.648	108.070	71.974	49.296	68.180	95.306
55	124.375	120.610	88.773	56.529	85.279	116.082
60	147.250	131.810	106.087	63.851	103.045	138.101
65	169.590	141.800	123.476	71.204	121.030	160.865
70	190.872	150.690	140.590	78.541	138.863	183.884
75	210.741	158.610	157.174	85.818	156.255	206.713
80	228.996	165.670	173.058	92.997	172.995	228.968
85	245.558	171.970	188.134	100.045	188.951	250.348
90	260.444	177.590	202.350	106.935	204.073	270.632
92	265.945	179.670	207.791	109.641	209.891	278.403
100	285.529	187.130	228.165	120.153	233.139	307.396
150	349.243	213.880	314.429	172.814	328.584	419.439
200	369.317	225.200	359.082	207.129	382.863	462.098
250	377.036	231.760	385.728	233.091	416.080	479.739
300	380.552	236.850	403.968	242.447	444.924	488.035

Table 7. Thermal conductivity of the tape's materials at various temperatures

T [K]	k_{Cu}	k_{Ag}	$k_{Hast.}$	k_{YBCO}	k_{NiW}	k_{SS}
5	157.700	11308.000	1.497	1.261	385.300	0.410
10	313.900	12846.000	2.695	2.740	385.300	0.924
15	462.600	8193.300	3.653	4.328	385.300	1.492
20	591.200	4889.300	4.424	5.774	385.300	2.068
25	684.300	3085.400	5.048	6.929	385.300	2.627
30	731.400	2075.400	5.557	7.727	385.300	3.156
35	734.500	1472.300	5.977	8.170	385.300	3.650
40	706.100	1144.000	6.327	8.303	385.300	4.107
45	661.200	935.590	6.622	8.200	343.900	4.530
50	611.400	798.480	6.873	7.945	307.800	4.919
55	564.000	705.590	7.092	7.608	277.300	5.278
60	522.400	641.070	7.284	7.231	252.000	5.610
65	487.800	595.280	7.456	6.807	231.600	5.917
70	459.900	562.140	7.611	6.261	215.500	6.201
75	438.000	537.710	7.754	6.002	203.000	6.467
80	421.100	519.390	7.887	5.782	193.200	6.715
85	408.200	505.400	8.013	5.588	184.900	6.948
90	398.400	494.520	8.132	5.421	176.800	7.167
92	395.200	490.850	8.178	5.360	173.300	7.251
95	391.100	485.920	8.247	5.276	167.400	7.375
100	385.800	478.980	8.357	5.152	156.600	7.573
150	375.000	446.390	9.372	4.649	114.100	9.225
200	379.100	432.520	10.340	4.617	98.890	10.726
250	381.100	424.400	11.290	4.553	92.020	12.401
300	380.800	419.490	12.230	4.745	90.000	14.420